PIXELS TO PYROMETRICS: UNCREWED AIRCRAFT SYSTEMS TO EVALUATE AND MONITOR PRESCRIBED FIRE

By Leo O'Neill

A Thesis

Submitted in Partial Fulfillment

of the Requirements for the Degree of

Master of Science

in Forestry

Northern Arizona University

December 2023

Approved:

Peter Z. Fulé, Ph.D., Chair

Andrea E. Thode, Ph.D.

Adam C. Watts, Ph.D.

ABSTRACT

PIXELS TO PYROMETRICS: UNCREWED AIRCRAFT SYSTEMS TO EVALUATE AND MONITOR PRESCRIBED FIRE

LEO O'NEILL

Prescribed fire is vital for fuel reduction and ecological restoration, though the effectiveness and fine-scale interactions are poorly understood. Uncrewed aircraft systems (UAS) coupled with infrared (IR) sensors present new opportunities for advancing prescribed fire science and evaluation. Here, I present three main chapters to introduce, research, and synthesize the concept of UAS-IR derived pyrometrics. The literature review chapter covers UAS for ecological monitoring, focusing on forest biometrics and fire pyrometrics. I describe the limitations of each and present a framework for understanding how these innovative technologies can improve our understanding of complex biophysical properties. As UAS-derived measurement accuracies improve, it is important to highlight the collaborative nature of these challenges; interdisciplinary collaboration will undoubtedly play a crucial role in future management practices. In the research chapter, I develop methods for processing UAS-IR imagery into spatially explicit pyrometrics: measurements of fuel consumption, rate of spread, and residence time to quantitatively measure three prescribed fires. I collected nadir IR imagery continuously (0.2 Hz) over a fixed area at three prescribed burns and one experimental calibration burn, capturing fire progression and post-frontal combustion for a total of 16 hours. Stabilizing the images with an Enhanced Correlation Coefficient model was robust against large perspective shifts and produced image stacks with less than one meter drift. UAS-IR fuel consumption correlated strongly with weight-based measurements of ten experimental burn plots, validating our approach to estimating consumption with a cost-effective UAS-IR sensor ($R^2 = 0.99$). UAS-IR pyrometrics of the three prescribed burns agreed with visual observations and showcased significant variability between each of the three fires. These findings demonstrate UAS-IR pyrometrics are an accurate approach to monitoring fire behavior and effects at spatiotemporal scales required to characterize prescribed fire. Additional research is needed to validate and compare against numerical, field-sampled standards. We noted that two of the three prescribed fires likely achieved consumption objectives, though objectives were often broad, unrealistic, and/or did not directly pertain to measured pyrometrics. Lastly, I synthesized the findings into a fact sheet tailored for fire and fuel managers. UAS-IR monitoring of prescribed fires is an accurate, efficient method of measuring fire. Refined fire monitoring coupled with refined objectives will be pivotal in informing fire management of best practices, justifying the use of prescribed fire, and providing quantitative feedback in an environment saturated with uncertainty.

ACKNOWLEDGEMENTS

I can't thank my community enough for supporting me during my research and schooling. Graduate school is no walk in the park and may be one of my most challenging, proud (soon to be) accomplishments. Honestly, the two seasons I spent as a hotshot were just as demanding as the two years in this program. With that, I would like the thank everyone that helped me. My partner Jasmine and my doggo (and coworker) Abi bore witness to all my successes and failures, I will forever be grateful for their support. My friends and family who never wavered to encourage me. Lionel and Sam for providing beer and wisdom. Lastly Dr. Fulé for advising me and my crazy ideas. This work would not be possible without the support from NAU School of Forestry, the CPS research team and the National Science Foundation, and Floyd Harding and the Salt River Project.

TABLE OF CONTENTS

LIST OF FIGURES

LIST OF TABLES

PREFACE

This thesis consists of and introduction, a literature review, a data-driven manuscript chapter, and a management implications chapter. All text in this thesis is written in first-person plural (“we”) to represent the collaborative effort of myself and co-authors or first-person singular (“I”) to reflect my personal ideas and experiences. Some content redundancy is present between chapters to comply with university thesis formatting guidelines.

Chapter 1 Introduction

In the Western US, wildfires are burning more area and at higher severities than most of the modern era (Singleton et al., 2019; Weber & Yadav, 2020). Wildfire risk has reached "crisis proportions" due to accumulating fuels, climate change, and an expanding wildland-urban interface (USDA, 2022). Under adverse climactic and forest conditions, wildfires are a top contributor to forest loss and vegetation type conversion (Abatzoglou & Williams, 2016; Prichard et al., 2021). However, designating all wildland fire as destructive and a threat to ecosystem resilience is an overgeneralization. Fire is an integral disturbance of many ecosystems (Bond & Keeley, 2005; Bowman et al., 2009). In fire-adapted forests such as those in the southwestern US, frequent fire was historically a driver of heterogeneous forest structure and age classes, maintaining low surface fuel loading and stand densities (Fulé et al., 1997; Hessburg et al., 2019). In response to shifting fire regimes, a primary objective of land management agencies is to increase forest resilience by reducing the buildup of fuels, an artifact of historical fire suppression policies (USDA, 2022). Hazardous fuel reduction often takes the form of mechanical fuel treatments, prescribed fire, or both to reduce the risk of severe wildfire. Despite the widespread use of prescribed fire to address the national wildfire crisis, studies investigating its efficacy have shown mixed results (Cansler et al., 2022; Fulé et al., 2012; Stephens et al., 2009; Waring et al., 2016).

Despite prescribed fire being one of two tools to address the wildfire crisis, our quantitative understanding of the effects is limited. Prescribed fire is a complex application of a biophysical process (fire), like a dosage, to arrive at a desired outcome (O'Brien et al., 2018). This presents an opportunity for unforeseen outcomes: intended application does not always yield intended effects. While prescribed fire is generally viewed as beneficial, studies investigating efficacy have shown mixed results (Cansler et al., 2022; Fulé et al., 2012; Hiers et al., 2016; Stephens et al., 2009; Waring et al., 2016). This necessitates a call for refined research studying the intricate patterns and processes of prescribed fire behavior and effects (Hiers et al., 2020). Improving our understanding and application of prescribed fire will be pivotal in informing fire management of best practices, justifying the use of prescribed fire, and providing quantitative feedback in an environment saturated with uncertainty.

Uncrewed aircraft systems (UAS) and new digital tools may serve to support prescribed fire management and research, as seen in other ecological applications (de Almeida et al., 2020; Jain et al., 2020). UAS can be rapidly deployed, easily operated, are relatively inexpensive, and are being adopted as a research and monitoring tool for ecological applications (Nitoslawski et al., 2021; Watts et al., 2010). Pyrometrics, the application of statistical, mathematical, and computational methods to characterize fire and fire effects, has undergone a transformation with the adoption of UAS and other sub-orbital remote sensing platforms (Nitoslawski et al., 2021).

UAS-derived data bridges the spatiotemporal gap between satellite sensors and field data, potentially providing a cost-effective method of monitoring and studying fine-scale prescribed fire patterns. Through the lens of fire and fuels management, machine learning and UAS-derived data form the nexus of the "digital forest."

This thesis aims to provide a comprehensive understanding of UAS-derived sensing of fire and fuel characteristics, organized into four chapters. Chapter two is a review of the literature on UAS and related platforms for fire and fuel measurements. Chapter three is a data-driven chapter to study the use of UAS for prescribed fire monitoring and evaluation, addressing two objectives: (1) validate the accuracy of UAS-based radiative energy surface fuel consumption estimates and (2) use extracted pyrometrics to characterize prescribed fire behavior and effects. Chapter three is a synthesis of chapter two into a two-page fact sheet, designed to inform managers of the implications of the research.

Chapter 2 The digital forest: UAS and big data as avenues to evaluate fire and fuels

1. Introduction

Uncrewed Aircraft Systems (UAS) occupy the fine-scale niche of remote sensing and serve as a catalyst for new ways to measure and understand fire and forest fuels. UAS "sense" (image, scan, sample) scenes at the 100 – 1,000-meter scale with very high temporal and spatial resolutions. They can be rapidly deployed, easily operated, are relatively inexpensive, and are rapidly being adopted as a research and monitoring tool for ecological applications (de Almeida et al., 2020; Manfreda et al., 2018; Watts et al., 2010). UAS are defined by the system (aircraft, control station, and control link) that carries a payload, but it is the payload, sensor or otherwise, that defines the application and utility of the UAS for remote sensing research (Nitoslawski et al., 2021). Common payloads are visible spectrum cameras (Chen et al., 2022), infrared sensors (Schumacher et al., 2022), laser scanners (Shin et al., 2018), multispectral sensors (Reilly et al., 2021), or a fusion of these sensors (Hartley et al., 2022). Advances in UAS and sensor technologies and a second wave of adopters applying these new tools for forest and fuels research have been a cornerstone in the "digital forest" (Nitoslawski et al., 2021).

UAS are part of a large adoption of remote-sensing innovations for ecological monitoring that provide the opportunity to study relationships and phenomena with big data (Nitoslawski et al., 2021). Data derived from UAS are on the order of megabytes to gigabytes, 1,000 times larger than the kilobyte scale of traditional forestry data such as plot-based measurements that characterize vegetation and fuel by sampling small plots to represent a population. This sampling approach can be time-consuming and may not reflect all conditions present at a heterogeneous study site. UAS-derived data can be sampled rapidly on short notice, providing wall-to-wall coverage of digital data that pair especially well with advanced models (Jain et al., 2020). The advantage of large datasets, big data, is the opportunity to apply machine learning to reveal complex interactions, signals, or phenomena (Jain et al., 2020). Big data's large sample size is essential to training and validating a local machine learning model, which would struggle to "learn" from smaller field datasets. Through the lens of fire and fuels management, machine learning and UAS-derived data form the nexus of the "digital forest." Common research themes include classification models to predict land cover, vegetation characteristics, and fuel conditions (Hillman et al., 2021; Krisanski et al., 2021; Moran et al., 2020); deep learning for fire detection (Chen et al., 2022; Shamsoshoara et al., 2021); and mixed methods to characterize fuels and fire behavior (Skowronski et al., 2020). Using machine learning to sift through the enormous volume of UAS-derived data, accuracies are comparable to (and sometimes surpass) field measurement counterparts (Donager et al., 2021; Hartley et al., 2022).

These broad themes in digital forestry, machine learning, and UAS, have undergone incredible strides in development in the last decade. The digital forest will likely continue to gain momentum with a steady increase in new publications (Nitoslawski et al., 2021). Here, I provide a comprehensive literature review of two emerging themes in forest and fuels UAS-based monitoring: biometrics and pyrometrics. This literature review highlights recent research that is pushing the bounds of forest and fuels monitoring using new technologies and how these advancements will help managers apply best practices to address complex ecological problems. Extracting metrics from UAS and other remote sensing sources is a challenging task that requires extensive interdisciplinary knowledge of processing, understanding, context, and assumptions.

2. Biometrics: forest and fuel characteristics derived from point clouds

Point clouds are three dimensional models presented as points with X, Y, and Z coordinates. Each point can have various attributes associated with it, such as RGB color, return intensity, classification, and time. While point clouds are commonly associated with light detection and ranging (lidar or laser scanning) sources, they are independent of the sensor and include other sources to describe forest structure: lidar, photogrammetry, and radar data (Bekar et al., 2021; Krisanski et al., 2018; Tinkham & Swayze, 2021). Point clouds are a data form used well before laser scanning and are not limited to lidar sensors (Levoy & Whitted, 1985). Interestingly, the first instance of using point clouds to describe laser scanning data wasn't until the early 2000's (Lim et al., 2003; Tseng & Wang, 2005), but laser scanning had been used to characterize forest structure since 1985 as waveform data (Nelson et al., 1984). Thus, the use of point clouds encompasses all data represented as three-dimensional point data. Below is a framework to understand the application and limitations to point cloud-derived biometrics. This framework can be condensed to three factors influencing biometrics: source and position of the point cloud, approach taken to derive metrics, and scale of the metrics.

2.1 Source and position

Point cloud source and position are the foundations of extracting accurate metrics. Discrete laser scanning and imaging cameras are the most common sources of points, though radar sensors for forest biometrics are under development (Bekar et al., 2021; Calders et al., 2020; Shin et al., 2018).

Laser scanning, as the title suggests, uses lasers to actively sense a subject. Each point is derived from an emitted laser pulse that contacts and is subsequently reflected off an object, so there is no preprocessing required to generate the point cloud. Laser pulses fractionally penetrate vegetation, recording the structure of the canopy (Lim et al., 2003). As the laser pulse contacts the forest canopy, a fraction of the energy is reflected to the scanner. The pulse continues to the ground where the remaining energy is reflected. The twofold benefit of sampling the ground and canopy makes lidar uniquely resistant to variability of forest density and structure (Donager et al., 2018).

Imaging cameras are inherently two-dimensional passive sensing, requiring preprocessing to generate point clouds (Iglhaut et al., 2019). Photogrammetry methods such as Structure-from-Motion (SfM) can estimate the critical "depth" attribute missing from images. SfM works by identifying tie-points, matching features present in multiple images, to generate a model of the imaged scene (Mahesh & Subramanyam, 2012). Tie-points are used to infer the position of the camera, inferring the "depth" attribute. Once images are aligned, a point cloud is generated, sometimes with comparable accuracies to laser scanning (Tinkham & Swayze, 2021). SfM point clouds are significantly cheaper than laser scanners because they can be generated with a consumer-grade camera, but they come with drawbacks. Camera specifications, image quality and quantity, and processing parameters all affect the accuracy of the point cloud (Swayze et al., 2021; Tinkham & Swayze, 2021). For example, a small set of low-resolution images at high altitudes processed with depth filtering will have significantly more positional error and lower point densities than optimal image sets and processing parameters (Swayze et al., 2021; Tinkham & Swayze, 2021). In addition, SfM is limited by visibility. Any objects visibly blocked in the images will not be represented in the point cloud, so dense canopies tend to occlude sub-canopy details and ground points (Belmonte et al., 2020; Swayze et al., 2021). While SfM is subject to more sources of error than laser scanning, many projects have successfully extracted forest and fuel biometrics (Hartley et al., 2022; Hillman et al., 2021; Krisanski et al., 2018; Moran et al., 2022; Shin et al., 2018). Using a UAS flying sub-canopy to capture images of a dense forest plot, estimates of diameter from the SfM point cloud were in strong agreement with field measurements (RMSE = 0.011 – 0.021 m) (Krisanski et al., 2020). Similarly, ground-based imagery (such as from phone cameras) and subsequent photogrammetric point clouds have corroborated this incredible accuracy estimating tree diameter (RMSE = 0.027 m) (Ahamed et al., 2023). Recent work using the color (spectral reflectance) attribute of points illustrates a unique application of SfM point clouds as compared to laser scanning to estimate metrics such as above ground biomass and tree crown scorch (Hartley et al., 2022; Moran et al., 2022). For example, Moran et. al (2022) used SfM-derived multispectral point clouds to discern between live and dead tree foliage to determine the height of tree crown scorch, with strong agreement with field measurements ($R^2 = 0.98$). With careful consideration and an optimal processing workflow, accurate SfM-derived biometrics can be achieved.

Point clouds can be sampled from terrestrial, airborne, and spaceborne sensors, though I focus on *in situ* positions: airborne and terrestrial. Airborne point clouds are most often acquired from a UAS or fixed-wing aircraft and terrestrial point clouds are sampled from scanners at a fixed position or with a mobile, handheld system. Scanner position can affect point cloud density, noise, and occlusion. Airborne point clouds are generally more sparse with higher positional error and occlusion of sub-canopy points (10 – 100 points/m^2) than terrestrially acquired data (100 – 1,000 points/m^2), but can cover a much larger extent (Donager et al., 2021). In a study comparing aerial and terrestrial laser scanning, aerial laser scanning from a fixed-wing aircraft flying at 1800 meters above ground had a reported vertical accuracy of 8.5 cm, versus the

1 – 3 cm accuracies of mobile laser scanning of the same location (Donager et al., 2021). While the point cloud quality was considerably affected, position had mixed effects on derived biometrics. Tree-scale metrics such as height, DBH, and detection were considerably less accurate from the aerial point clouds, but plot-scale metrics such as density, basal area, volume, and biomass were robust to impacts from position (Donager et al., 2021).

Research studying how point cloud source and position affects derived biometrics is seldom in agreement. If an aerial SfM point cloud has sub-canopy occlusion and more spatial error than laser scanning, would derived canopy cover and tree height necessarily be less accurate? Few papers have compared multiple sources, positions, and field measurements in a controlled environment (Brede et al., 2019; Chamberlain et al., 2021; Donager et al., 2018, 2021; E. Hyyppä et al., 2020; Shin et al., 2018). When comparisons are made, the approach and scale are most often different. For example, Donager et. al (2021) and Calders et. al (2015) made methodologically similar comparisons of estimated tree heights from terrestrial point clouds with field data, but found considerably different outcomes. Donager et. al (2022) found terrestrial point clouds underestimated tree heights (n = 159, RMSE = 3.3 m), but Calders et. al (2015) concluded a similar practice was very accurate (n = 61, RMSE = 0.55 m). In fact, Calders et. al (2015) found that using a laser hypsometer was significantly less accurate than point cloud derivatives, true height determined by cutting the tree down and measuring stem length with a tape (RMSE = 1.28 m). The discrepancy of these two papers is likely attributed to different processing steps and forest structure. Both papers used the same approach, comparable lidar scanners, and measured tree height directly from the point cloud. The tree density in Calders et al. (2015) plots were around 300 tree/ha, whereas Donager's plots ranged from 25 – 1,300 trees/ha. An earlier paper that used the same point cloud data as Donager et al. (2021) noted there was significant point occlusion from laser acquisition (Donager et al., 2018). Compared to Calder's study, each plot was sampled with one fewer scan and each scan was 30 meters farther apart than Calders' study (Calders et al., 2015; Donager et al., 2018). Two nearly identical studies in design and target metric had notably different findings due to the quality of the scan and approach. Most studies place terrestrial laser scanning point clouds as the most likely to return accurate metrics (Calders et al., 2015; Donager et al., 2018, 2021; E. Hyyppä et al., 2020). Ultra-high resolution terrestrial point clouds have been shown to surpass metric accuracies of their traditional counterparts, such as above ground biomass and available fuels (Calders et al., 2022; Hartley et al., 2022).

Aerial laser scanning is comparable to terrestrial-based point clouds, but approach and forest structure should be considered before generating "challenging" sub-canopy metrics (Donager et al., 2021; E. Hyyppä et al., 2020). Structure-from-Motion derived point clouds are appealing as a cost-effective monitoring tool, but they are limited in use due to canopy occlusion (Cook, 2017). With SfM, all that is needed is a consumer-grade camera, typically on the order of hundreds of US dollars. Lidar sensors and equipment needed to process the data can be significantly more expensive than a camera for photogrammetry (White et al., 2013). Most research using UAS SfM advises users to consider the limitations and drawbacks and if their target metric can be accurately sampled (Belmonte et al., 2020; Krisanski et al., 2020; Shin et al., 2018; Tinkham & Swayze, 2021).

2.2 Scale

Scale refers to the spatial dimensions of the area being studied. Scale is divided into tree- (0.01 h), plot- (0.1 – 1.0 ha) and stand-scales (10 – 100 ha) for the purpose of point cloud processing (Donager et al., 2021). Height, diameter at breast height (DBH), canopy base height, location, and biomass are all common tree-scale metrics derived from point clouds (Krisanski et al., 2021). Plot-scale metrics include height, basal area, density, canopy cover, canopy bulk density, and biomass (Chamberlain et al., 2021). Finally, stand-scale metrics include patch size and patch density (Donager et al., 2021). Plot-scale metrics are often derived from area-based approaches, though individual tree-based approaches can be summarized for each plot. Plot-scale metrics are the most robust to other variability in point cloud biometrics and are often similar to field metric counterparts (Donager et al., 2021). The primary pitfall of tree-scale metrics is the influx of error that comes with individual tree detection algorithms (Donager et al., 2021). Bias is introduced when suppressed and dominant trees have omission and commission errors, respectively.

2.3 Processing approach

Biometrics extracted from point clouds can be delineated by the general approach taken to process the point cloud. Directly analyzing millions of points is computationally expensive, so researchers have developed various approaches to efficiently extract metrics (Iglhaut et al., 2019). The most common approaches are area-based (Packalen et al., 2019) and individual tree-based (Tinkham & Swayze, 2021), though other approaches such as point-based (Vega et al., 2014), voxel-based (Bienert et al., 2014), and data-driven (Whelan et al., 2023) may become established as popular metric extraction approaches given more development (Maltamo et al., 2014).

An area-based approach summarizes point cloud metrics for defined extents, such as a grid, polygons, or plots. In each unit, the point cloud data is summarized and is often represented as a raster. Mean and maximum point height, standard deviation of heights, canopy cover, and canopy base height are a few metrics that are used in an area-based approach. Area-based approaches can also include models to derive target metrics. Plots with a given metric, such as above ground biomass, are modeled using an array of point cloud summary statistics (Hartley et al., 2022). The area-based approach is the simplest way to extract metrics from point clouds and well-proven in ecological monitoring uses (Packalen et al., 2019), but other approaches have been found to be significantly more accurate (Whelan et al., 2023).

The individual tree-based approach summarizes point cloud metrics using trees as the experimental unit (J. Hyyppä & Inkinen, 1999). Using individual tree detection (ITD) to classify points associated with each identified tree, metrics are summarized for each tree's point cloud. The tree-based approach has excellent crossover with traditional field measurements. For example, tree height and diameter at breast height can be estimated using the tree-based approach and traditional methods. One major pitfall to ITD-based approaches is that any omission or commission errors of the initial tree detection classification will have residual effects on the remainder of the analysis. Smaller trees and dense, multi-age forest stands can have high omission rates, biasing the results towards larger, dominant trees (Donager et al., 2018; Shin et al., 2018).

A point-based approach uses each point as the experimental unit of a point cloud. It is computationally expensive and hard to extract forest biometrics without inferential models. Since most forest biometrics are at the plot- and tree-scale, point-based metrics are summarized similar to area- and tree-based approaches. Point-based approaches retain all dimensions of the data and show potential to be effective at fine-scales (Krisanski et al., 2021; Vega et al., 2014).

Voxels, a concatenation of "volumetric pixels", are another approach that preserves the height attribute of point clouds while aggregating, rather than raster two-dimensional aggregation. Voxels are essentially boxes in space that summarize their contents based on user specifications. For example, a 1 m^3 voxel may include 100 points from an RGB point cloud. While the size and position of the voxel are pre-defined, the metrics derived from the points can be resampled by any summarizing statistic: standard deviation, mean, median, etc. The mean color attributes, median point classification, and standard deviation of height values for all the points are a few examples of summaries that can be extracted from the point cloud (Whelan et al., 2023).

A data-driven approach uses zero-order metrics, which are basic statistical measures calculated directly from the point cloud. Zero-order metrics could include: the mean of height returns, the percentage of voxels that contain given point densities, or the maximum skewness of point return intensity to develop a model (Hillman et al., 2021; Whelan et al., 2023). While a data-driven approach may use voxels, rasters, or other data type similar to other approaches, this method focuses on developing a localized model rather than generalized metrics (Bright et al., 2022; Fernández-Guisuraga et al., 2022). For example, Hartley et al. (2022) took a data driven approach to model above ground biomass and available fuels in a highly flammable forest type in New Zealand. Using a random forest regression model, they found that structural metrics such as point cloud height distributions were the best predictors of aboveground biomass (R^2 0.89, RMSE 18.6%). In fact, UAS-derived point cloud metrics outperformed non-destructive field metrics (R^2 0.44, RMSE 34.5%). A significant caveat to this finding and the data-driven approach taken is that the model is localized to the study site, the model would need to be retrained to be accurately applied in another location or fuel type.

Many projects use multiple approaches to derive metrics or employ a hybrid of two approaches. While classifying approaches can be subjective, approach has a tangible effect on metric accuracies, as seen in the Donager et al. (2021) and Calders et al. (2015) reviews described earlier. Moran et al. (2020) used an area approach to extract first and second-order biometrics from aerial laser scanning point clouds of select western forests. Then, these metrics trained a gradient boosting machine using Landsat-derived indices to predict the point cloud-derived metrics. This study applied an area-based approach then a data-driven approach to model forest and fuel characteristics, outperforming LANDFIRE spatial data. For example, predicted canopy height correlated much better with observed height measurements when using Moran's model ($R^2 = 0.67$) than LANDFIRE ($R^2 = 0.156$) (Moran et al., 2020; Reeves et al., 2009). Area-based approaches are fairly resistant to changes to point cloud density, source, and position, and deliver accurate first order metrics, given the limitations of the point cloud (Donager et al., 2018; Packalen et al., 2019). To derive metrics at the tree scale, an individual tree-based approach is often taken, though tree-detection algorithms often require fine-scale parameterization and loose accuracy as forest density and structure complexity increases (Donager et al., 2021; Tinkham & Swayze, 2021).

2.4 Point cloud framework

A significant portion of research focusing on biometric extraction from point clouds has focused on ground truthing metrics for accuracy assessments (Bienert et al., 2014; Calders et al., 2015, 2022; Chamberlain et al., 2021; Donager et al., 2021; Krisanski et al., 2018, 2021; Lim et al., 2003; Shin et al., 2018; Terryn et al., 2022; Whelan et al., 2023). Accuracy assessment research is the foundation to effectively applying point cloud-derived biometrics to other studies focusing on the processes and fluxes of forest ecosystems. The process of biometric extraction from point clouds can be understood with a framework. The three main factors affecting biometric accuracy are source and position, approach, and scale. All point clouds have utility, though the source and position will significantly affect the subjective *quality* of biometrics. Depending on the approach and scale taken to extract metrics, point clouds with more positional error and occlusion may still return comparable biometrics to field measurements or more costly point cloud sampling methods. Regardless of the point cloud, caution should always be taken when considering the accuracy of point cloud-derived biometrics.

3. Pyrometrics: fire kinematics and effects

The term pyrometrics has technical meanings in ceramics, metallurgy, thermodynamics, and more recently, fire ecology. *Pyro*(fire)*metrics*(measurements) refers to the application of statistical, mathematical, and computational methods to characterize fire and fire effects (Perrakis et al., 2019). The fundamentals of pyrometrics have been in practice as early as the 20th century when fire ecology was formalized as a discipline. The concept of pyrometrics aims to provide a basis for understanding and studying fire and effects, supporting fire and fuel management decision making, and unify a growing field of research. In this section, I discuss the development of new approaches to generating pyrometrics and the subsequent ripple effects transpiring in fire management and modeling.

3.1 Fire monitoring with UAS-IR

Pyrometrics derived from infrared (IR) sensors is undergoing a “renaissance” (Moran et al., 2019)- from theoretical and experimental research to practical application (Dickinson et al., 2016; Hudak et al., 2020; Johnston et al., 2018; Loudermilk et al., 2012; O’Brien et al., 2015; Paugam et al., 2021; Schumacher et al., 2022; Valero et al., 2021). UAS, infrared sensors, and advanced geoprocessing are the cornerstones of this movement to digitize fire monitoring. Recently, research has applied experimental work in deriving pyrometrics from sub-orbital remote sensing platforms and produced accurate, spatially explicit measurements of fine-scale fire patterns and processes (Moran et al., 2019, 2022; Schumacher et al., 2022). Pyrometrics derived from UAS-borne infrared imagery includes energy release (Moran et al., 2022) and rate of spread (Gowravaram et al., 2022; Moran et al., 2019; Schumacher et al., 2022) though this list is likely to grow as UAS-IR imagery becomes more widely available and easier to process.

Consumption and energy release estimates from infrared imagery have long been tested in laboratory and experimental settings (Freeborn et al., 2008; Kremens et al., 2012; Wooster, 2002). These experiments using IR imagery provided the foundation for our understanding of energy released in the form of radiative heat, called fire radiative power (FRP). Additionally, laboratory testing and small experimental burns found a strong relationship between biomass consumed and fire radiative energy (FRE, integrated FRP) (Freeborn et al., 2008; Kremens et al., 2012). For example, Kremens et al. (2012) studied the total energy budget of consumption and found that FRE accounted for ~17% (S.D. = 0.03) of all energy released during combustion of *Quercus* litter and wood. Aerial (piloted aircraft) infrared imagery from an experimental broadcast burn used calorimetric research of wood consumption (Reid & Robertson, 2012) and the fraction of radiative energy from Kremens et al. (2012) to develop a generalized formula (Equation 5 in Chapter 3) for estimating consumption with airborne and thermal imagery (Hudak et al., 2016; O’Brien et al., 2015). This method, however, has not been applied to UAS-IR imagery. Moran et al. (2022) extracted FRE from UAS-IR imagery and found a moderate correlation between FRE and crown scorch of a prescribed fire (Spearman rank correlation = 0.43).

Three pitfalls of UAS-IR consumption and energy release pyrometrics are evident in recent research: canopy occlusion, fuel moisture, and temperature saturation. When sensing with a UAS positioned above tree tops, surface fuel energy release is occluded by the presence of canopy cover. This presents a challenge for inferring consumption of surface fuels under dense canopies. While studies have corrected for this occlusion at the plot scale, this method remains unvalidated and cannot be applied to high-resolution estimates of energy release (Hudak et al., 2016). Occlusion was a significant source of uncertainty during Moran's (2022) study to relate FRE to crown scorch for individual trees. Moran et al. (2022) masked FRE pixels occluded by tree canopies, but if the tree had a large canopy, much of the sub-canopy fire energy could not be measured. Fuel moisture may also lead to inaccuracy in UAS-IR pyrometrics. When Kremens et al. (2012) studied the energy budget of combustion, they used 12 plots with variable fuel loading, wood to litter ratios, and moisture representative of typical burn conditions. While there was no discussion of the effect of fuel moisture on their results, the plots with low pre-fire fuel moisture generally had a lower fraction of radiative energy than the high moisture plots, 14% and 21%, respectively. Fundamentally, a unit of fuel will emit less radiative energy than the same unit of fuel that is drier. More latent energy is required to vaporize (dehydrate) the fuel as part of bringing it to ignition temperature, the first step of pyrolysis. In other words, increasing fuel moisture reduces the released radiative energy, FRE. Other lab tests have corroborated that increasing fuel moisture is linearly related to decreasing FRE per unit of biomass consumed (Smith et al., 2013). Despite these challenges, UAS-IR imagery of consumption offers an alternative to measuring consumption with conventional methods that is spatially explicit. In lab tests, nadir IR sensors performed remarkably well to predict fuel consumption ($R^2 > 0.8$) (Freeborn et al., 2008; Kremens et al., 2012; Smith et al., 2013; Wooster, 2002). In the field, consumption derived from aircraft-IR predicted observed consumption from aggregated clip plots relatively well, with some underestimation noted ($R^2 = 0.48$) (Hudak et al., 2016). To date, no field study has used UAS-IR to estimate fuel consumption while accounting for variability in fuel moisture affecting the fraction of fire radiation per unit of fuel consumed. Lastly, it is important to address the limitations of IR sensors to accurately measure remarkably high temperatures present during biomass combustion. Saturation refers to the highest temperature at which a sensor can accurately measure. Above this point, the sensor cannot differentiate between temperatures and may provide inaccurate readings. Long-wave infrared sensors often saturate below the accepted maximum of instantaneous flaming combustion, 1,100° C (Martin et al., 1969; Wotton et al., 2012). If these temperatures exceed the saturation temperature of the infrared sensor, the readings may not be reliable. This can lead to underestimation of the energy produced, which is critical to precisely estimating energy release of combusting biomass via FRE. While this limitation should be acknowledged, most prescribed fire typically involves low intensity fire, which is well below the maximum combustion temperature and IR saturation temperature (Iverson et al., 2004; Kennard et al., 2005). Additionally, the alternative to infrared sensing, thermocouples, are prone to underestimating the upper reaches of combusting temperature due to their thermal mass causing a lag in rapid temperature changes (Kennard et al., 2005).

Estimating rate of spread (RoS) has been a target of recent pyrometric research (Johnston et al., 2018). Many studies take a stationary nadir approach to sample the thermal imagery- a natural opportunity to use UAS as the sensor platform (Gowravaram et al., 2022; Johnston et al., 2018; Moran et al., 2019; Sagel et al., 2021; Schumacher et al., 2022). As consumer-grade, inexpensive platforms become available with radiometric cameras, the cost of operating a UAS and collecting imagery on wildfires has been dramatically reduced relative to crewed aircraft research (Manfreda et al., 2018). Generally, stationary UAS-IR image stacks are collected on short time intervals (0.2 – 10 seconds) to monitor the flaming front RoS. The images are converted to temperature, stabilized, and then analyzed using a vector-based approach (Gowravaram et al., 2022; Moran et al., 2019; Schumacher et al., 2022). For example, Moran et al. (2019) dissolved the progression map to polygons and sampled the closest point from consecutive polygon edges. Schumacher et al. (2022) used a moving window that calculated correlations between two consecutive images. The best correlation for each bounding box area was inferred to be progression of the flaming zone, a proxy for RoS. This approach produces a spatially explicit raster where each pixel is a velocity estimate of the fire front. Results from these studies are promising, but none of the three UAS-IR studies validated or ground-truthed their estimates (Gowravaram et al., 2022; Moran et al., 2019; Schumacher et al., 2022). In an experimental test, Johnston et al. (2018) compared several methods of estimating ROS and found the approach had a strong influence on the results. Out of eight approaches tested, a vector-based method similar to the UAS-IR approaches discussed above, was most similar to a conventional method, thermocouple arrays ($R^2 = 0.77$) (Johnston et al., 2018).

Fire monitoring with UAS-derived infrared imagery has garnered notable research attention. Lab-tested relationships, equations, and approaches developed 10+ years ago are being applied to operational and experimental broadcast burns. While results are promising, significant preprocessing and validation is required to generate pyrometrics. Future research should focus on improving UAS-IR pyrometrics by accounting for factors such as canopy occlusion and fuel moisture, as well as validating various processing approaches.

3.2 UAS-IR supported fuel management

In the Western US, wildfires are burning more area and at higher severities than most of the modern era (Singleton et al., 2019; Weber & Yadav, 2020). Wildfire risk has reached “crisis proportions” due to accumulating fuels, climate change, and an expanding wildland-urban interface (Hurteau et al., 2014; USDA, 2022). Under adverse climactic and forest conditions, wildfires are a top contributor to forest loss and vegetation type conversion (Abatzoglou & Williams, 2016; Prichard et al., 2021). However, designating all wildland fire as destructive and a threat to ecosystem resilience is an overgeneralization. Fire is an integral disturbance of many ecosystems (Bond & Keeley, 2005; Bowman et al., 2009). In fire-adapted forests such as those in the southwestern US, frequent fire was historically a driver of heterogeneous forest structure and age classes, maintaining low surface fuel loading and stand densities (Fulé et al., 1997; Hessburg et al., 2019). In response to shifting fire regimes, a primary objective of land management agencies is to increase forest resilience by reducing the buildup of fuels, an artifact of historical fire suppression policies (USDA, 2022). Hazardous fuel reduction often takes the form of mechanical fuel treatments, prescribed fire, or both to reduce the risk of severe wildfire. Despite the widespread use of prescribed fire to address the national wildfire crisis, studies investigating its efficacy have shown mixed results (Cansler et al., 2022; Fulé et al., 2012; Stephens et al., 2009; Waring et al., 2016).

Prescribed fires have objectives to be achieved. By manipulating the seasonality, weather conditions, and firing pattern of the prescribed fire, managers can manipulate the outcomes to match the objectives, a practice that has much more potential to be informed by research than full-suppression wildfire operations (Hiers et al., 2020). Prescribed fire objectives are often broad in scope and challenging to evaluate with traditional monitoring practices, raising the question of whether achieving objectives results in the desired outcome (Lutes et al., 2006). In some cases, first and second entry prescribed fires are not achieving objectives in a southwestern ponderosa forest (Waring et al., 2016). While burning does reduce fire hazard (Cansler et al., 2022; Fulé et al., 2012), the anticipated degree to which it is reduced by prescribed fire is not typically evaluated. Many managers lack the capacity, technical experience, and funding to maintain a fire monitoring program (Lutes et al., 2006). UAS-IR fire monitoring could be a key factor in bolstering prescribed fire monitoring and research efforts.

Prescribed fire behavior is influenced by factors at much finer scales than wildfires, limiting the use of orbital remote sensors (Hiers et al., 2020; Manfreda et al., 2018). Complex fire-fuel interactions are represented best by spatially explicit two- and three-dimensional relationships, so traditional fuels and fire monitoring are unable to capture fine-scale heterogeneity that is the driver of prescribed fire outcomes (Hiers et al., 2020). UAS-IR fire monitoring delivers fine-scale, spatiotemporally explicit pyrometrics ideal for prescribed fire research. Operationally, UAS-IR pyrometrics could be used in fire monitoring programs to evaluate if prescribed fire objectives are achieved. With validation and streamlined processing, data from UAS-IR has the potential to revolutionize how fine-scale fire is monitored and evaluated, much as laser scanning has done for biometrics. While implementing UAS-IR in fire monitoring programs is likely a few years away, hardware and software will continue to improve, making UAS-IR a critical factor in adapting and responding to the wildfire crisis.

3.3 UAS-IR to inform fire models

Modeling and understanding how vegetative fuel conditions interact with (relatively) static topographic factors and incredibly dynamic weather scenarios to govern fire behavior has been a target of research and management for decades. Though current fire models serve as the primary tools for fuel management planning, they are not designed to model prescribed fire behavior (Parsons et al., 2023). Next-generation prescribed fire models need to function at fine scales, account for complex ignition patterns, and offer actionable results for fire managers. Rather than focusing on the risk to firefighters or the likelihood of the fire escaping containment features, prescribed fire models may focus on the ecological effects of the burn or the smoke emissions (Hiers et al., 2020; Parsons et al., 2023). As new fire models are coming available and managers are focusing on addressing wildfire risk with informed prescribed fire, UAS-IR may serve as a data source to validate and calibrate new physics-based models (Hiers et al., 2020).

QUIC-Fire is a physics based fire-atmospheric model, meaning it uses three-dimensional data to model physical processes (Parsons et al., 2023). QUIC-Fire coupled with FastFuels, a database of landscape voxelized fuels, are platforms capable of modeling at fine scales for prescribed fire behavior and effects (Hiers et al., 2020; Parsons et al., 2023). FastFuels can be thought of as a "superhighway" modeling platform, where wall-to-wall data coverage is already present for the US and "on-ramps" are available so areas can be updated with other sources of three-dimensional data, such as UAS-derived lidar (Parsons et al., 2023). While development is underway to provide QUIC-Fire with relevant and easy to use fuels data, no platforms are presently available to inform and validate the fire component of the model. Processed UAS-IR imagery could serve to as calibration and validation data for fire-atmosphere models that require high-resolution, spatially explicit data. UAS-IR imagery combined with pre- and post-fire UAS SfM or laser scanning acquisitions could be used as plot-scale case studies of these fire and fuel models for relatively low cost of operation.

4. Conclusion

Advancements in biometrics and pyrometrics have been catalyzed by the accessibility of new technologies and collaboration of disciplines. The innovative approaches detailed in this literature review are cost-effective, easy to apply, accurate, and deliver results often unachievable using traditional methods. While adoption and use of UAS-derived data is owed largely to accessibility, it is critical to highlight the human element, especially in an era characterized by artificial intelligence and automation. Addressing complex forest and fire challenges will undoubtedly utilize accessible technologies, but interdisciplinary collaboration will shape the innovative approach and play a crucial role in future management practices.

Chapter 3 Pixels to pyrometrics: UAS-derived infrared imagery to evaluate and monitor prescribed fire behavior and effects

Abstract

Prescribed fire is vital for fuel reduction and ecological restoration, though the effectiveness and fine-scale interactions are poorly understood. Uncrewed aircraft systems (UAS) coupled with infrared (IR) sensors present new opportunities for advancing prescribed fire science and evaluation. Here, we develop methods for processing UAS-IR imagery into spatially explicit pyrometrics, measurements of fuel consumption, rate of spread, and residence time to quantitatively measure three prescribed fires. We collected nadir IR imagery continuously (0.2 Hz) over a fixed area at three prescribed burns and one experimental calibration burn, capturing fire progression and post-frontal combustion for over three hours, in some cases. Stabilizing the images with an Enhanced Correlation Coefficient model was robust against large perspective shifts and produced image stacks with less than one meter drift. UAS-IR fuel consumption correlated strongly with weight-based measurements of ten experimental burn plots, validating our approach to estimating consumption with a cost-effective UAS-IR sensor ($R^2 = 0.99$). UAS-IR pyrometrics of the three prescribed burns agreed with visual observations and showcased significant variability between each of the three fires. Our findings demonstrate UAS-IR pyrometrics are an accurate approach to monitoring fire behavior and effects at spatiotemporal scales required to characterize prescribed fire. Additional research is needed to validate and compare against numerical, field-sampled standards. We noted that two of the three prescribed fires likely achieved consumption objectives, though objectives were often broad, unrealistic, and/or did not directly pertain to measured pyrometrics. Refined fire monitoring coupled with refined objectives will be pivotal in informing fire management of best practices, justifying the use of prescribed fire, and providing quantitative feedback in an environment saturated with uncertainty.

Keywords

fire behavior, fuel consumption, fire monitoring, fire radiative energy (FRE), fire radiative power (FRP), fire rate of spread, image stabilization, infrared imagery, prescribed fire, uncrewed aircraft systems (UAS), unmanned aerial vehicles (UAV)

1. Introduction

In the Western US, wildfires are burning more area and at higher severities than most of the modern era (Singleton et al., 2019; Weber & Yadav, 2020). Wildfire risk has reached “crisis proportions” due to accumulating fuels, climate change, and an expanding wildland-urban interface (Hurteau et al., 2014; USDA, 2022). Under adverse climactic and forest conditions, wildfires are a top contributor to forest loss and vegetation type conversion (Abatzoglou &

Williams, 2016; Prichard et al., 2021). Though, designating all wildland fire as destructive and a threat to ecosystem resilience is an overgeneralization. Fire is an integral disturbance of many ecosystems (Bond & Keeley, 2005; Bowman et al., 2009). In fire-adapted forests such as those in the southwestern US, frequent fire was historically a driver of heterogeneous forest structure and age classes, maintaining low surface fuel loading and stand densities (Fulé et al., 1997; Hessburg et al., 2019). In response to shifting fire regimes, a primary objective of land management agencies is to increase forest resilience by reducing the buildup of fuels, an artifact of historical fire suppression policies (USDA, 2022). Hazardous fuel reduction often takes the form of mechanical fuel treatments, prescribed fire, or both to reduce the risk of severe wildfire. Despite the widespread use of prescribed fire to address the national wildfire crisis, studies investigating its efficacy have shown mixed results (Cansler et al., 2022; Fulé et al., 2012; Stephens et al., 2009; Waring et al., 2016).

Prescribed fires differ from wildfires in three aspects: they are intentional and planned, interact at fine scales, and are designed to achieve specific outcomes. During the planning phase, managers can manipulate the burn conditions (seasonality, firing pattern, weather) to achieve specific prescription objectives, such as reducing dead and down fuel loadings and understory vegetation, retaining dominant trees and snags, and modifying forest structure and composition to the natural range of variability (Fernandes & Botelho, 2003; Fulé et al., 2012; Reynolds et al., 2013; Ryan et al., 2013; Waring et al., 2016). The planning and outcome of prescribed fires has much more potential to be informed by research than full suppression wildfire operations, due to the fact that burns are conducted with the intention of achieving a desired prescription (Hiers et al., 2020). While much research is focused on wildfires, there is a growing need for research using spatially explicit tools to understand prescribed fire processes and quantitatively inform land management on treatment effectiveness and best practices (Hiers et al., 2020).

Fire behavior is a complex effect of many interacting agents, one being fuels (Hudak et al., 2020; O'Brien et al., 2018; Parsons et al., 2017). The spatial pattern of fuel is a multiscale property, heterogeneous at fine (< 1 m^2) and coarse (>1 m^2) scales (Loudermilk et al., 2012; Rowell et al., 2020). Consequently, submeter fuel variability is linked to submeter fire variability. While this spatial scale is critical for understanding ecological fire effects and processes (O'Brien et al., 2018), traditional point- and area-based fuels and fire monitoring are unable to capture the detail needed to characterize these complex fire and fuel patterns (Hiers et al., 2020). Additionally, fire behavior is often sampled by observing fire, such as estimating rate of spread by timing the fire front's progression between points of known distances (Rothermel & Deeming, 1980). This approach is limited to observations of low intensity fire spread near the perimeter that are not occluded by smoke, resulting in inevitable sampling bias. Coupled with recent advances in characterizing fine-scale vegetation structure and composition, spatially explicit, fine-scale measurements of fire behavior will present new opportunities to study the complex patterns and processes of prescribed fire (Hoffman et al., 2018; Rowell et al., 2020).

Uncrewed Aircraft Systems (UAS) and new digital tools may serve to support prescribed fire management and research, as seen in other ecological applications (de Almeida et al., 2020; Jain et al., 2020). Pyrometrics, the application of statistical, mathematical, and computational methods to characterize fire and fire effects, has undergone a transformation with the adoption of UAS and other sub-orbital remote sensing platforms (Nitoslawski et al., 2021). Pyrometric research using UAS and piloted aircrafts draws upon theoretical and lab-tested work to produce spatially explicit measurements of fine-scale fire patterns and processes (Bright et al., 2022; Hudak et al., 2016; Moran et al., 2019, 2022; O'Brien et al., 2015; Schumacher et al., 2022). Pyrometrics derived specifically from UAS-borne imagery include energy release (Moran et al., 2022), rate of spread (Gowravaram et al., 2022; Moran et al., 2019; Schumacher et al., 2022), tree crown scorch (Moran et al., 2022), burn severity (Hillman et al., 2021), and fire behavior interactions (Filkov et al., 2021). UAS-derived data bridges the spatiotemporal gap between satellite sensors and field data, potentially providing a cost-effective method of monitoring and studying fine-scale prescribed fire patterns.

Using infrared imagery to measure fire energy release, rate of spread, and other fire behavior characteristics is common in fire ecology research (Johnston et al., 2018; Kremens et al., 2012; Mathews et al., 2016; Sagel et al., 2021; Smith et al., 2013; Wooster et al., 2005). Most of these studies though, are limited to the laboratory setting or experimental burns where ample time is provided to set up equipment in a semi-controlled environment and cameras are mounted in fixed positions. For rate of spread, measurements derived from IR imagery compare well with thermocouple estimates of spread, though accuracies depend on temperature thresholds and the algorithm to extract IR-derived rate of spread (Johnston et al., 2018). Infrared imagery can be used to estimate fuel consumption with two approaches appearing in literature (Hudak et al., 2016; Smith et al., 2013). Both approaches use a radiometrically calibrated infrared image stack of the entire combustion process, convert temperature or reflectance to power using equations similar to the Stefan-Boltzmann law, and then integrate power over time to calculate energy release. Converting radiative energy released to fuel consumed using a generalized algorithm has been done accounting for varying energy densities of fuels (Hudak et al., 2016; Kremens et al., 2012) or variable moisture of the fuel consumed (Smith et al., 2013). With the onset of UAS, using infrared imagery to measure fire behavior is presented with a new set of opportunities and challenges. Consumer-grade UAS are cost-effective, accessible, and can be easily deployed for fire monitoring use. Conversely, UAS-borne (and similar crewed platforms) infrared sensors often have a low saturation threshold, so maximum fire temperatures may not be measured (Moran et al., 2019). The imagery is unstable and requires colocation and registration pre-processing (Valero et al., 2021). UAS often are limited in flight time, so post-frontal combustion may be omitted (Moran et al., 2022). Pyrometrics derived from UAS and similar crewed platforms have shown promise to be a viable source of pyrometric data, though derived measurements are seldom validated. Recent research continues to be tool-centric, developing the processing protocol to calibrate, stabilize, georeferenced, and extract metrics from aerial infrared imagery. This tool-centric research is critical prior to applying it for studying fire ecology, such as assessing the accuracy of UAS-infrared imagery to estimate fuel consumption. The next evolution of UAS-derived pyrometrics remains relatively unstudied: using refined pyrometrics to characterize fire and understand biophysical patterns and processes in modes not possible using traditional sampling practices.

We initiated this study to evaluate if UAS can be used to quantitatively monitor and measure prescribed fire. We collected UAS-derived radiometric long-wave infrared (LWIR) imagery of a calibration experimental burn and three prescribed fires to (1) validate the accuracy of UAS-based radiative energy surface fuel consumption estimates and (2) use extracted pyrometrics (consumption, rate of spread, and residence time) to characterize prescribed fire behavior and effects. We expected UAS-derived infrared (IR) imagery would be an accurate approach to estimating surface fuel consumption and that extracted pyrometrics would match visual estimates of fire behavior and characterize the variability, if any, between and within each prescribed fire.

2. Methods

These methods describe the workflow we developed to acquire images using an IR-equipped UAS (2.1), preprocess the images into calibrated and georeferenced raster stacks of radiative power and energy (2.2), test and validate approaches to convert radiative energy to fuel consumption (2.3), apply the workflow to UAS-derived IR imagery collected of prescribed fires to extract pyrometrics consumption, rate of spread, and residence time (2.4), and analyze the results to address our research objectives (2.5 and 2.6). With modification, these methods can be applied to IR image sets that capture fire behavior at fine temporal sampling rates.

2.1 UAS Platform and imagery collection

All UAS imagery was collected with an Autel Evo II 640t UAS, featuring a 48-megapixel color camera and a 0.32-megapixel IR camera. The thermal camera is an Infiniray Micro III Lite 640 (Yantai, Shandong, China) uncooled radiometric sensor that sampled at the longwave IR wavelengths, 8 – 14 µm with a temperature range of 0° – 650° Celsius. The UAS and cameras are consumer-grade, meaning they are relatively inexpensive to operate, easy to maintain, and accessible to purchase.

Immediately prior to ignition operations, we launched the UAS to collect images of the fire behavior. We positioned the UAS directly overhead the center of the plots, facing north and at 122 m above ground, and collected thermal imagery at 0.2 Hz (five second interval) to capture ignitions and post-frontal fuel consumption. With a realistic flight time of 30 minutes, five batteries, and field charging array, we could perpetually hover the UAS. About every 30 minutes, we paused thermal image sampling to swap the UAS battery, returning to the same altitude and location to resume monitoring. It is important to note we used the low gain setting to capture infrared images, which is less sensitive than the high gain but can sense at the full operational range of the camera. Biomass combustion occurs across a range of temperatures, exceeding 1,100° C in some cases (Martin et al., 1969; Wotton et al., 2012). While the LWIR sensor used in this project saturates below the maximum potential combustion temperature (Moran et al., 2019; Paugam et al., 2013) and is subject to flame emissivity dependence on flame depth (Johnston et al., 2014), we selected this camera because of its affordability and simple use. Saturation refers to the highest temperature at which a sensor can accurately measure. Above this point, the sensor cannot differentiate between temperatures and may provide inaccurate readings. Sensor saturation can lead to underestimation of the energy produced, which is critical to precisely estimating energy release of combusting biomass via IR sensing. While this limitation should be acknowledged, most prescribed fire typically involves low intensity fire, which is well below the maximum combustion temperature and IR saturation temperature (Iverson et al., 2004; Kennard et al., 2005).

2.2 Thermal Imagery Preprocessing

The thermal imagery acquired from the UAS in raw form was a 16-bit 1-band raster, with no geolocation information. Without appropriate processing, quantitative spatial analysis would not be possible. We processed imagery in three steps, detailed in this section: conversion to temperature, stabilization, and georectification. All pyrometrics were derived from infrared imagery were preprocessed using the methods described below, similar to Moran et al. (2019, 2022) and using equations developed and applied by O'Brien et al. (2015) and Hudak et al. (2016, 2015).

We used a blackbody calibration source to convert the 16-bit digital numbers to temperature in degrees Celsius. The 16-bit pixel values ranged from 2,800 for the cold regions of the frame to 6,000 for intense flaming areas. We chose not to carry out conversion using Autel's proprietary software because it used the compressed .jpeg thermal images and had no batch processing functionality. Instead, we used a blackbody calibration source to develop an algorithm to convert the thermal imagery from the uncompressed .tiff images. Using the blackbody, we tested the thermal camera using the full range of the calibrator: between 0° – 100° Celsius at 5-degree increments. The results of this bench testing confirmed the accuracy of the radiometric IR sensor and were used to develop a linear conversion algorithm (Figure S3.4).

Equation 1

$$f(x) = 0.0982x - 268.39$$

where x is the IR sensor's reported digital number and $f(x)$ is the calibrator temperature, which explained the relationship well ($R^2 = 0.99$). We applied this equation to convert the .tiff pixel digital numbers to calibrated temperature.

Next, we stabilized the imagery. The stabilization process coregisters each image so that drift such as positional and rotational movement are removed from the images. The process of orthorectifying thermal imagery of fire is challenging, and research to provide an open-source solution is ongoing (Moran et al., 2019; Paugam et al., 2021; Valero et al., 2021). We used OpenCV (Bradski, 2000) and Python to test four transformation algorithms and the use of a fire mask to stabilize the thermal image stacks. The models we selected for testing have been used to coregister images for this type of application or were demonstrated to outperform a model previously tested for this application (Mahesh & Subramanyam, 2012; Valero et al., 2021). We tested: KAZE, Scale-Invariant Feature Transform (SIFT), Enhanced Correlation Coefficient-based (ECC) with an affine transformation, and ECC with a homography transformation (Alcantarilla et al., 2012; Evangelidis & Psarakis, 2008; Lowe, 1999). To generate the transformation matrix of images, we used an iterative method that compares image i to image $i+1$. A transformation matrix is then applied to each respective image after a buffer has been calculated, shifting images based on their transformation to maintain the true ground position x,y. The KAZE and SIFT algorithms use a Random Sample Consensus algorithm to generate a homography transformation. Additionally, we tested an affine and a homography transformation for the ECC algorithm. Affine transformations preserve parallel lines and ratio of distances, but a homography transformation is more adaptive to other forms of motion, such as perspective shifts. We used a sample image stack (Hundred Rx plot 2) thermal image stack to test each transformation algorithm. With ~9,000 infrared images, manual georectification was not possible. Therefore, to evaluate the transformation models, we manually selected the location of the ground control points (GCPs) of 30 images to compare to the first image of the image stack. Then, the positional distance of selected pixels from reference pixels was calculated as:

Equation 2

$$d(p_1, p_2) = \sqrt{(p_{1x} - p_{2x})^2 + \left(p_{1y} - p_{2y}\right)^2}$$

where $d(p_1,p_2)$ is the Euclidian distance between points p_1 and p_2 and each point is broken down into their respective x and y pixel coordinates. We used the ECC model with an affine transformation to stabilize all thermal imagery hereafter.

After image stabilization was complete, we georeferenced the image stacks using the locations of four GCPs visible in the thermal images (GDAL/OGR Contributors, 2023). Transform matrices were generated manually for the first images and applied to all the stabilized images. If the plot was sampled for more than an hour or there was a visible shift or distortion in the stabilization process, the images were divided into sub-stacks, where the first image of each stack was georeferenced. To validate the final result of the stabilization and georeferencing process, we selected 30 images from each plot image stack incrementally, representing the entire duration of the image stack. Then, we manually identified visible GCPs in each image. The coordinate location of each selected point was compared to the true location of the nearest GCP using Equation 1 to calculate the distance error after processing. The Root Mean Squared Error (RMSE) was calculated for each plot using the average distance error of each of the thirty images sampled.

Once the images were georectified and converted to temperature, we processed the image stack from temperature to measurements of energy and power. To do this, we converted the radiant temperature of each pixel to fire radiative power (FRP; W m^{-2}) using the Stephan-Boltzmann law for grey body emitters, applied similarly in Hudak et al. (2018):

Equation 3

$$FRP = \epsilon\sigma(\mathrm{T}_{\mathrm{i}}^4 - T_{bi}^4)$$

where ϵ is the emissivity of the grey body, σ is the Stephan-Boltzmann constant ($5.67*10^{-8}$ W m^{-2} K^{-4}), T is radiant temperature (Kelvin), and T_b is the background temperature (Kelvin). We used an emissivity constant of 0.98 (López et al., 2012; Moran et al., 2019; O'Brien et al., 2015). We elected to use a background temperature equal to as the 10th percentile of pixel temperatures for each raster image. The background temperature (T_b) accounts for changes in surface temperatures from solar radiation during multi-hour IR image collection. 10th percentile background temperatures were often near 300 K, the background temperature used by Hudak et al. (2018).

We approximately integrated pixel-scale measurements of FRP to calculate fire radiative energy (FRE; MJ m^{-2}) using the trapezoidal rule (Hudak et al., 2016, 2018), effectively converting power to energy:

Equation 4

$$FRE \approx \frac{1}{2}\sum_{\mathrm{i}=1}^{\mathrm{n}}(\mathrm{FRP}_{\mathrm{i}} + \mathrm{FRP}_{\mathrm{i}-1}) \cdot (\mathrm{t}_{\mathrm{i}} - t_{\mathrm{i}-1})$$

where consecutive FRP rasters are integrated over time, t (seconds). We used the trapezoidal rule to integrate FRP because some image stacks had pauses in collection. While images were sampled every five seconds, there were some breaks in data collection when batteries were exchanged or, in the case of two plots, periods when there was little change in fire spread or energy release.

Canopy cover, where present, occluded nearly all the thermal radiation from surface fuel consumption below the canopy. Since the surface fuels were heterogenous, we removed the sub-canopy FRP pixels by masking any pixels that did not reach a radiative power of 1,070 W m^{-2} (Hudak et al., 2016).

2.3 Experimental calibration burn

We conducted an experimental burn to validate the estimates of surface fuel consumption derived from a UAS-mounted LWIR sensor and equations 3 – 4. To do this, we burned known quantities of ponderosa fuel and measured the consumption directly by weighing fuel before and after the burn (hereafter weight-based) and compared it to consumption estimates derived from the UAS infrared imagery (hereafter UAS-based). Images were processed as described in section 2.4 to generate FRE of each plot. Then, we calculated fuel consumption using two published estimators (Equations 5 and 6) and compared it with consumption calculated by weighing fuel before and after. This calibration burn compared the UAS IR method of estimating consumption with a validated, ground-truth counterpart in a variety of fuel conditions.

Ten 1-m^2 plots were marked with paint on bare ground. Seven of the same aluminum GCPs used for monitoring the prescribed fires were placed around and between the plots. We precisely weighed and homogeneously arranged variable amounts of dry ponderosa litter and cut logs (~35 cm length and 12 cm diameter) in each plot. We selected coarse woody debris (CWD) and litter quantities that are representative of fuel conditions encountered in ponderosa forests (Table 3.1). Roccaforte et al. (2012) reported a maximum 10 kg m^{-2} and 0.8 kg m^{-2} of CWD and litter loadings, given the bulk density of litter is ~4 Mg ha^{-1} cm^{-1} (Stephens et al., 2004). We doubled each of these quantities to account for the spatial heterogeneity typical of surface fuels. Fuel moisture was sampled immediately prior to ignitions from three wood and three litter samples and calculated as the relative loss of water content after drying in an oven at 70°C for 24-hour intervals until the dry weight was stable.

Plots were ignited with a flare to avoid adding fuel and energy to the plot during ignition. We collected IR imagery at 0.2 Hz, 100’ above ground for two hours and 15 minutes. Consumption was immediately stopped by spraying all the plots with water and extinguishing any smoldering. After the burn, all remaining ash and charred wood was collected, dried in an oven at 70° C until the weight stabilized, and weighed to calculate the total consumption, accounting for fuel moisture.

Table 3.1: Calibration burn fuel loading, actual consumption measured in the field (weight-based), and estimated UAS consumption (UAS-based) using the Smith et al. (2013) of each 1-m^2 plot designed to represent fuel loading conditions encountered in southwestern ponderosa forests.

Plot	Dry wood weight (kg)	Dry litter weight (kg)	Fuel moisture	Weight-based consumption (kg)	UAS-based consumption (kg)	Percent consumption (weight-based)	Percent consumption (UAS-based)
1	1.83	0.43	11%	2.14	2.44	95%	108%
2	3.48	0.89	11%	4.30	4.29	98%	98%
3	5.36	1.78	11%	7.00	7.19	98%	101%
4	7.18	0.45	11%	7.49	8.22	98%	107%
5	8.93	0.90	11%	9.64	10.64	98%	108%
6	10.74	1.78	11%	12.26	12.15	98%	97%
7	12.53	0.45	11%	12.70	13.51	98%	104%
8	14.26	0.89	11%	14.67	15.95	97%	105%
9	16.06	1.78	11%	17.50	18.19	98%	102%
10	17.79	1.78	11%	19.07	21.54	97%	110%

We compared methods for fuel consumption (FC) estimation using two different FRE-based approaches:

Equation 5 (Hudak et al., 2016)

$$FC = FRE/rf/hc$$

Equation 6 (Smith et al., 2013)

$$FC = \frac{FRE}{(3.025 - 5.32 * W_c)}$$

where consumption is *FC* (kg m^{-2}), *hc* is heat content (MJ kg^{-1}), *rf* is radiative fraction, and W_c is water content (percent). Equation 5 is an energy density-based approach that accounts for the heat content of the fuel and the proportion of energy released radiatively (Hudak et al., 2016). We used an *rf* of 17%, the average radiative fraction of the 12 *Quercus* litter and woody debris experimental burns carried out by Kremens et al. (2012). The heat content for all ponderosa fuel components was 20.86 MJ kg^{-1} (Van Wagtendonk et al., 1998). Equation 6 comes from Smith et al. (2013). This moisture-based approach does not account for the effect of variable heat contents of fuel types and instead addresses the strong effect moisture has on radiative fraction and consumption (Smith et al., 2013).

To compare UAS-based fuel consumption approaches, we used the orthogonal distance regression with respect to the 1:1 line, which minimizes the sum of perpendicular distances. This method considers errors in both the independent (weight-based consumption observations) and dependent (UAS-based consumption predictions) variables by calculating the residuals as the perpendicular distance from the regression line. We used the orthogonal distance to calculate the error of points to evaluate the performance of each approach relative to the theoretical linear 1:1 relationship we expect observed and predicted consumption to exhibit.

2.4 Prescribed fire imagery acquisition and analysis

We collected data at three operational prescribed fires, two in Arizona and one in Florida (Table 3.2). The prescribed fire sites were all composed of a fire tolerant *Pinus* species but displayed substantial variability in fuel loading, fire seasonality, and target fuel load reductions (Table 3.2). To collect data on prescribed fires in Arizona, we obtained permission from the USDA Regional Fire and Aviation Office to operate UAS and coordinated with local US Forest Service districts to attend approved prescribed fires. In Florida, the prescribed fire was on private land and we coordinated with landowners to attend the fire. We adhered to the Federal Aviation Administration Part 107 rules and the safety regulations written in the US Forest Service research contract (when attending agency-administered prescribed fires). Sites were selected based on availability of prescribed fires during the 2022 – 2023 season. Prescribed fires were ignited in the Fall, Winter, and Spring and were within the target weather window described in the prescribed burn plans (S3.1 – S3.3).

Prior to ignitions, we located plots that were representative of the fuel conditions of the prescribed fire sites. We placed plots near the perimeter of the fire, typically on opposite sides of the burn unit to capture multiple plots during one ignition operation. Plot size of the thermal imagery was variable, dependent on the UAS altitude, drift, and stability. Generally, plots were about 0.4 ha (Table 3.2). We placed four 40-cm diameter aluminum pans in each plot, one in the center and three in the north, south, and west directions about 15 – 20 m from the center pan (prioritizing canopy openings to avoid occlusion). The pans acted as ground control points (GCPs), allowing us to continually fly the UAS over the same location, georectify images, and validate the georectification. Shiny aluminum contrasted the forest floor well and had a low emissivity, meaning the plates were clearly visible in the infrared and color imagery. We used the pans to georectify the thermal image stacks and verify that the stabilization and coregistration workflow produced acceptable results, as described below. At the Hanna Hammock Rx, we geolocated each pan using a real-time kinematics GPS with centimeter-level accuracy. At the Hundred Rx and Wild Bill Rx, we measured the distance between each GCP and inferred their coordinate position by orthorectifying pre-burn images of the plot via photogrammetry (Agisoft, 2023). This method was centimeter-level accurate as well, but the precision of the plot location was subject to the precision of the UAS GPS. We recorded the average daily fuel moisture of 10-

hour fuels from the nearest Remote Automated Weather Station, available from the Western Regional Climate Center (http://www.raws.dri.edu)

We used the best performing method from the calibration burn, the moisture-based approach (Equation 6), to convert FRE to consumption for the prescribed fire plots. One challenge with monitoring with UAS is capturing post-frontal combustion (Moran et al., 2022), which may continue for hours or days after the burn. We balanced collecting as many plots as possible with capturing all possible post-frontal consumption by sampling about two plots per operational shift, each plot being sampled until radiant energy release had substantially subsided. To estimate post-frontal combustion, we fit a linear regression with a logarithmic transformation of the average plot FRP at each infrared image collection time. Linear regressions were calculated for each burn:

Equation 7

$$ln(FRP) = \beta_0 + \beta_1 \times Time + \epsilon$$

We fit the linear regression to the energy release from the peak energy release to the end of the image capture, which visually exhibited a logarithmic relationship. Then, we used this model to predict unmeasured energy release of the plots from when data collection stopped to when the theoretical energy release ≤1 W m^{-2}. Comparing the total energy (FRE) measured with the predicted unmeasured energy release gave us a corrective factor, which we applied to each consumption raster to account for any unmeasured energy. For example, if the regression predicted 20% of energy was not captured during collection, then each pixel would be multiplied by 1.2.

To estimate rate of spread, we used the masked FRP raster stack to generate an arrival time, or progression, raster of the fire when each pixel reached flaming power, 1,070 W m^{-2} (Hudak et al., 2016). Then, rate of spread was derived as the rate of change, or slope, of the progression raster (Moore et al., 2020) using the equation:

Equation 8

$$ROS = \frac{1}{\tan(slope)} \times 60$$

where ROS is measured in m min^{-1}. The slope raster was then converted to points and interpolated for all progression pixels using inverse distance weighing. Residence time was calculated as the total time (in seconds) that each pixel was greater than or equal to 300 degrees Celsius (Wotton et al., 2012).

Table 3.2: Site names, location, fuel and forest characteristics, and plot and imagery processing metadata.

Site	**Location (elevation, m)**	**Date**	**Forest type**	**Est. fuel load (Mg/ha)**	**Avg. Fuel Moisture (%)**	**No. of plots**	**No. of images (IR/RGB)**	**IR image location error (RMSE, m)**	**Avg. thermal sampling time (min)**	**Avg. plot size (m^2)**
Calibration Burn	35.173°, -111.653° (2,100)	Sept., 2023	Experimental	25 – 220	11	10	1,500	0.10	142	1
Hanna Hammock Rx	30.660°, -84.250° (60)	Feb., 2023	Longleaf Pine	5.7*	15	2	800/400	1.93	38	4,500
Hundred Rx	34.148°, -110.813° (2,000)	Apr., 2023	Ponderosa Pine	34 – 45**	4.2	2	1,600/800	1.01	71	3,900
Wildbill Rx	35.322°, -111.783° (2,400)	May & Jun., 2023	Ponderosa Pine		5.9	4	5,500/1,400	1.24	152	4,100

* Tall Timbers research program (Bigelow et al., 2023)
** Tonto National Forest 2023 Burn Plan (S3.2)

2.5 Visual observations

We visually observed fire behavior and recorded qualitative descriptions of each of the prescribed fire plots: rate of spread, intensity, residence time, and fire direction. We used this data to make comparisons between the IR-derived fire metrics and our estimate of fire behavior of each burn to determine if estimated and observed fire metrics agreed. While this approach is subjective to the observer, relative differences in fire behavior of each burn could be characterized and compared with UAS-IR pyrometrics as a general indicator of approach performance.

2.6 Statistical analysis

To evaluate the effectiveness of UAS-IR imagery at capturing the "signal" of prescribed fires, we needed to determine if the spatial resolution was adequate for measuring heterogeneity of fire behavior. In signal processing, the Nyquist criterion states the sampling interval (or resolution in this case) should be twice that of the frequency in the sample (Hengl, 2006; Shannon, 1949). So, we evaluated the resolution of the "signal" to determine the resolution needed of the sensor. For example, if the signal was Lego color and the sensor was a microscope, the optimal resolution would be half that of (or less) the Legos. The microscope "images" would have significant spatial autocorrelation present, illustrating the sensor is much finer than needed to capture the signal. We constructed a semi-variogram of each plot's FRE raster to determine the spatial scale at which autocorrelation was no longer significant. Then, we calculated the median semi-variogram range of all the plots and resampled each pyrometric raster to this value. We checked for autocorrelation using Moran's I test to confirm that the resampling did in fact reduce autocorrelation. This resulted in pyrometric rasters of the burns where each pixel is spatially independent. This enabled us to do spatial analysis at the pixel scale to determine if the UAS-IR sensor resolution and process described above of extracting pyrometrics is sensitive enough to detect changes between each prescribed fire. For each prescribed fire, we aggregated the resampled pixels from all the plots, representing the three pyrometrics extracted. Using the resampled replicates (pixels) for each group (prescribed fires), we employed a Kruskal-Wallis test to determine if any pyrometric was significantly different between each burn: consumption, rate of spread, and residence time. The Kruskal-Wallis test was suitable for our data because it does not assume normality. If the Kruskal-Wallis test indicated significant differences, we used the Dunn test, a post-hoc test for non-parametric data, to determine specifically which burns were different from one another.

3. Results

We successfully collected 16 hours of imagery of fire behavior, stabilizing and processing it into spatially explicit pyrometrics from three prescribed fires and one calibration burn. The average plot size of the thermal imagery was 0.41 hectares and the average duration of fire captured was 87 minutes (Table 3.2). The longest duration of thermal imagery was 3.5 hours, captured at plot 3 of Wild Bill.

Using Hanna Hammock plot two imagery, we tested the performance of stabilization models and a fire/no-fire mask for removing positional and rotational drift from the thermal image stacks (Figure 3.1). The SIFT algorithm with a fire pixel mask performed the best, stabilizing the image stack with a median Euclidian error (Equation 1) of 3.5 pixels (SD = 1.1). Nonetheless, we used the second-best performing stabilization model, the ECC-affine transformation (median = 11.1, SD = 3.4), to stabilize all the plots for analysis because it was notably more robust to large changes between images, such as perspective shifts from interruptions in sampling for battery replacements, wind, and rapid fire growth. All plots were processed with the ECC-affine stabilization model with no mask for further analysis.

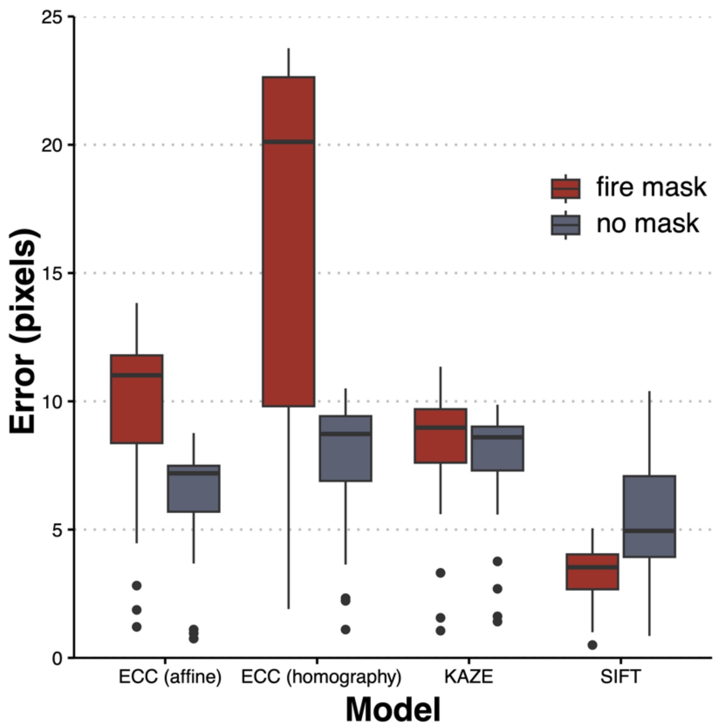

Figure 3.1: Error of the stabilization models tested: Enhanced Correlation Coefficient (ECC) with an affine transformation, ECC with a homography transformation, KAZE, and Scale Invariant Feature Transform (SIFT). Each model was tested with and without a mask that removed flaming areas. Error was measured using the Euclidian distance (Equation 2) of GCPs of image *i* relative to the first image (reference image) in 30 selected images from the stabilized image stack.

3.1 UAS-derived Consumption

Observed weight-based consumption of the ten 1-m^2 plots ranged from 2.1 – 19 kg m^{-2} with all plots consuming 95% or more of dry-weight fuel (Table 3.1). We measured average litter and wood fuel moisture as 9.6% and 12%, respectively. UAS-based consumption estimates were in high agreement with observations across all plots, as illustrated in Figure 3.2. Converting radiative energy using either Equation 5 or 6 to consumption was highly correlated with observed consumption. However, Equation 5 from Hudak et al. (2016) consistently underpredicted consumption. The linear regression had a slope of 0.75 (R^2 = 0.99, RMSE = 0.38) and the mean orthogonal error from the 1:1 line was -1.9 kg m^{-2}. Converting FRE using the fuel moisture approach from Smith et. al (2013), Equation 6 was closer to a 1:1 relationship with a linear regression slope of 1.1 (R^2 = 0.99, RMSE = 0.54) and an average orthogonal error with respect to the 1:1 line of 0.52 kg m^{-2}. Therefore, all our estimates of consumption for the prescribed fires (Table 3.2) were generated with the Smith et al. (2013) equation (Equation 6).

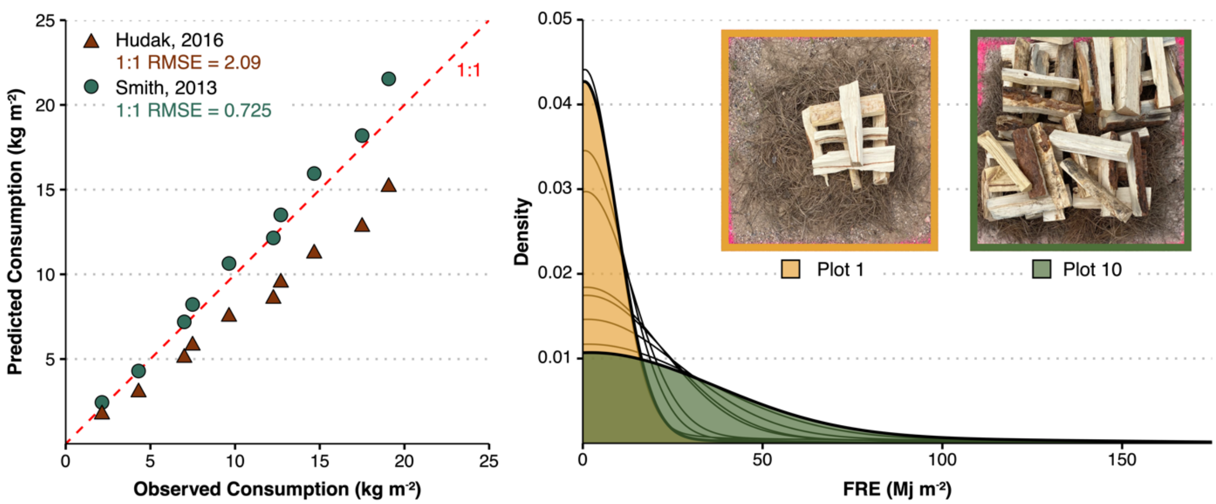

Figure 3.2: Calibration burn results from weight-based measurements of consumption and UAS-based consumption (left plot). Brown points (triangles) use Equation 5 from Hudak et. al (2016) and green points use Equation 6 from Smith et al (2013). Root Mean Square Error was calculated with the orthogonal distances between points and the 1:1 line to account for error of the weight-based consumption observations. The density plot (right plot) highlights the variability of FRE pixels of plot 1 (left image) and 10 (right image), with remaining plots represented as lines.

3.2 Prescribed fire visual observations

We visually observed low severity fire consuming ground and surface fuels at each of the prescribed fires (Figure 3.3). Of the fires, the Hanna Hammock Rx had the highest observed intensity with a few instances of crown scorching, high rates of spread (> 8 m min^{-1} at peak), and head fire with flame lengths up to 1 m. We observed lower intensities at the Hundred Rx and

Wild Bill Rx: rates of spread (< 2 m min^{-1}) and fire front flame lengths (< 0.5 m) were low with the fire backing and flanking while consuming coarse woody debris. Post-frontal residence time (> 30 min) was longer and fuel consumption was higher at Wild Bill and Hundred burns as many of the plots had large amounts of coarse woody debris present (Figure 3.3a). Much of the fuel at Hanna Hammock was fine (litter, shrubs, and small sticks), so post-frontal combustion was on the order of minutes rather than hours like the burns in Arizona.

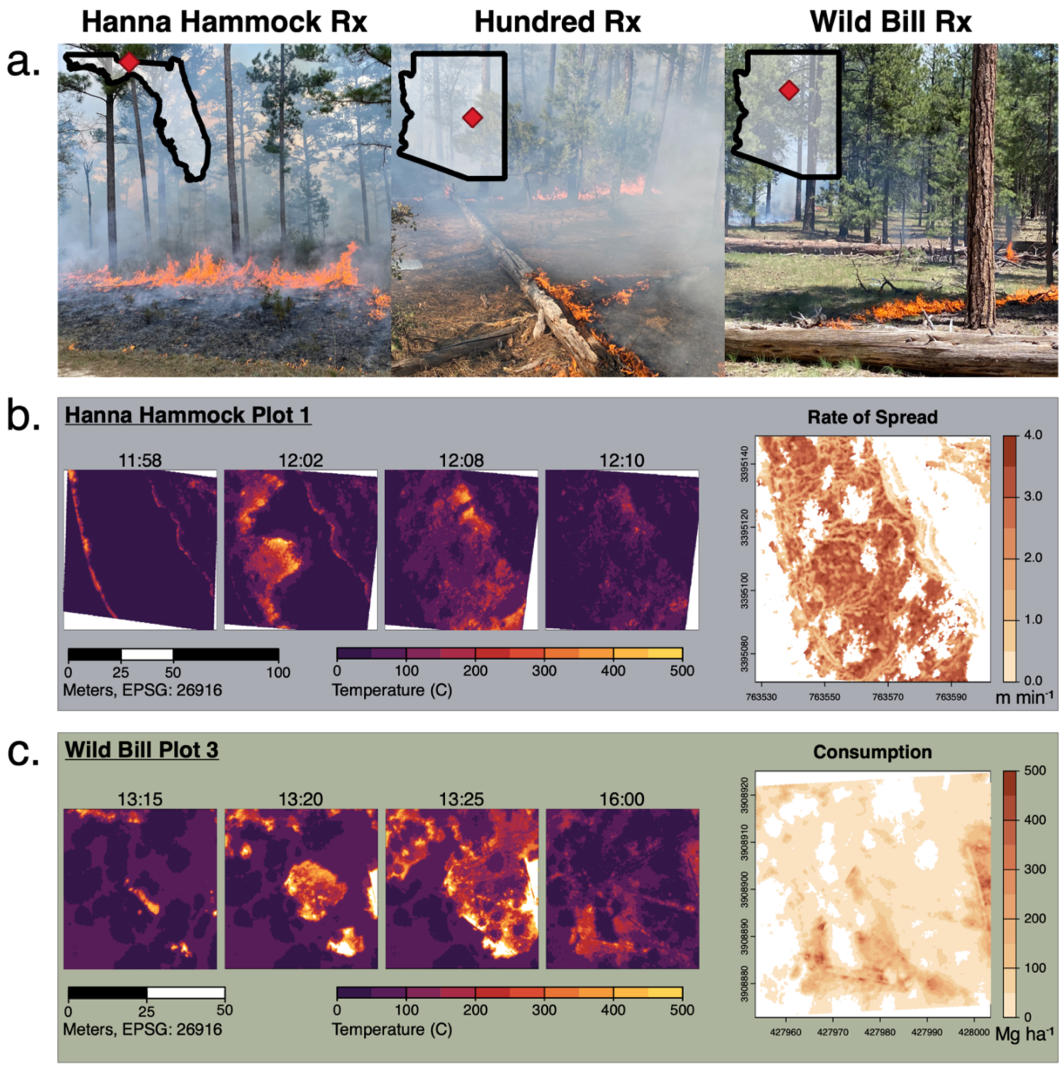

Figure 3.3: Location and images of fire behavior of the prescribed fires monitored (a), selected IR images and derived rate of spread raster of the Hanna Hammock plot 1 (b), and selected IR images and derived consumption raster of the Wild Bill plot 3 (c). Hanna Hammock Rx had the highest visually observed rate of spread and lowest consumption. Wild Bill Rx had a significant amount of coarse woody debris present in plots and had the highest visually observed estimate of consumption and residence time.

3.3 UAS-IR fire behavior

Extracted pyrometrics from the UAS-derived IR imagery agreed with visual observations of the burns: Hanna Hammock spread the fastest (median and peak) and Hundred and Wild Bill prescribed fires consumed more fuel with longer residence times. Predicted FRE using Equation 7 to account for unmeasured FRP performed well, with strong model fits with the captured energy (Figure 3.4). Plots where the UAS imagery collection captured enough post-frontal combustion that a decay curve was evident had the strong model performance. At the Hanna Hammock plots, majority of the energy was released within 10-minutes, so most energy was measured with the UAS and only a fraction was modeled with the regression equation. The prescribed burns in Arizona continued to release significant energy for hours after the peak FRP in some cases, so accounting for unmeasured energy released at these burns was critical for estimating total energy released and consumption. Total consumption for Hanna Hammock, Hundred, and Wild Bill were 3.0, 13.7, and 49.2 Mg ha^{-1}, respectively. The consumption data was heavily positively skewed (Figure 3.5). Maximum within-plot consumption was 650 Mg ha^{-1}, sampled at plot 1 of the Wild Bill Rx. Median rate of spread was 2.5, 0.7, and 0.7 m min^{-1} for Hanna Hammock, Hundred, and Wild Bill prescribed fires, respectively. Rate of spread reported by the UAS imagery ranged from 0.002 – 4.0 m min^{-1}, the maximum recorded at plot 1 of Hanna Hammock and the minimum recorded in plot 4 of Wild Bill prescribed fire. Median residence time was 40, 96, and 170 seconds for Hanna Hammock, Hundred, and Wild Bill prescribed fires, respectively.

Using a semi-variogram to identify autocorrelation for each plot´s radiative energy (FRE) raster, we found the median range to be 4.6 m. Before resampling, FRE rasters of each plot had a median resolution of 0.13 m (Table 3.2) and Moran’s I value of 0.96, indicating a very strong positive autocorrelation. This means that about 35 pixels (4.6 m resolution) were resolved into one to minimize autocorrelation. Therefore, the Nyquist sampling theorem would suggest a sampling resolution of 2.3 meters or less is needed to characterize the fire behavior of prescribed fires. After spatial resampling (to 4.6 meters), median Moran’s I was reduced to 0.29: while spatial autocorrelation was still present, it was markedly reduced. A Kruskal-Wallis test of the resampled pyrometric data showed that each pyrometric had significantly different groups (Figure 3.5). The post-hoc Dunn tests showed that Wild Bill and Hundred groups were similar in terms of rate of spread or residence time distributions (Figure 3.5), though all other Dunn tests were significant (p-value < 0.025).

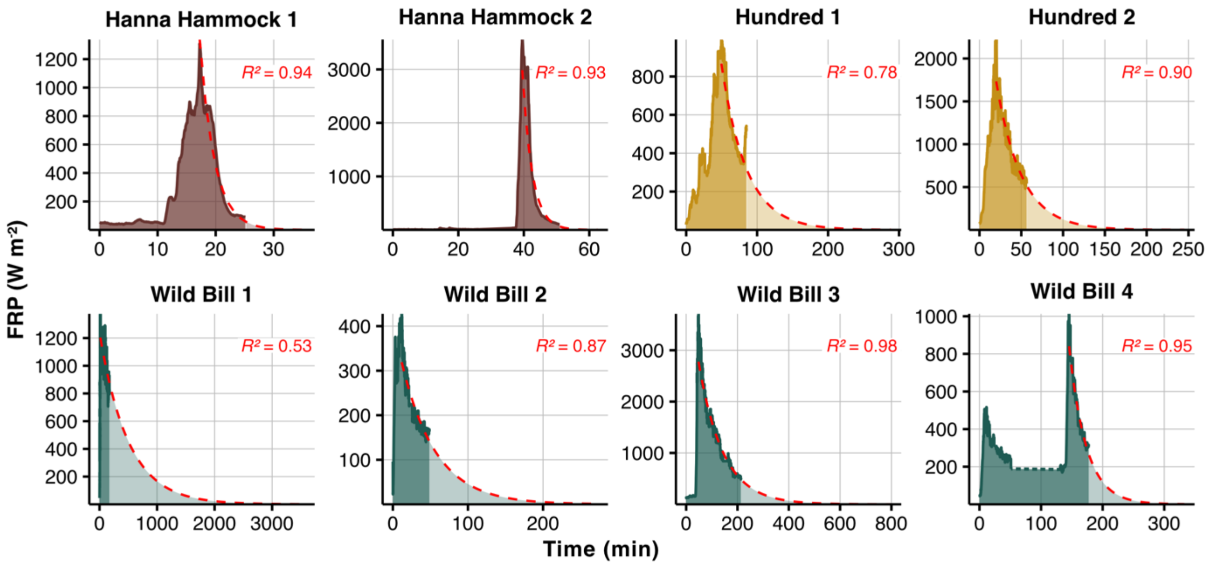

Figure 3.4: Fire radiative power (W m^{-2}) over time of each of the burn plots. Red dashed line is the logarithmic transformed linear regression and respective R^2 values denote model performance evaluated with measured energy data. Dark shaded area is the energy measured by the UAS-IR imagery, lightly shaded area is unmeasured energy predicted using the regression, which we accounted for in the final consumption estimates. The green fine-dashed line in Wild Bill 4 plot represents a long pause (~1 hr) in imagery collection during minimal, static fire activity. This particular plot was burned in early morning when conditions were relatively cool and wet, so fire intensity was particularly low. Then, ignition operations made a second pass at minute 150 corresponding to the spike in fire radiative power.

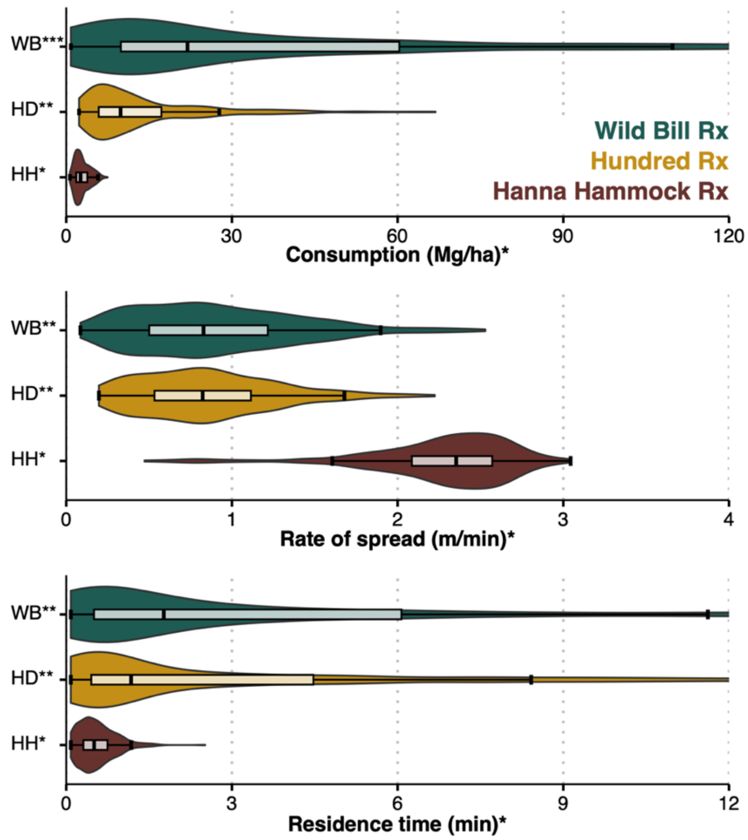

Figure 3.5: Violin distributions and boxplots of UAS-derived pyrometrics from each prescribed fire: Hanna Hammock Rx, Hundred Rx, and Wild Bill Rx. A significant Kruskal-Wallis rank sum test that two or more of the distributions are different is marked as an asterisk on the x-axis label. Post-hoc Dunn tests to determine pairs of significantly different distributions are marked as asterisks on the burn labels.

4. Discussion

The preprocessing workflow developed to calibrate, stabilize, and georeference UAS-IR imagery was effective for deriving pyrometrics. We converted LWIR emittance to temperature using a bench-tested algorithm (Equation 1) that performed well ($R^2 = 0.99$). Then, we selected the ECC-affine transformation model to stabilize image stacks with sub-meter drift. Finally, we georeferenced image stacks using GCPs with one meter-level precision (average RMSE = 1.1 m).

Our calibration experiment demonstrated that estimating fuel consumption using UAS-IR imagery was accurate in a range of fuel loading conditions and could be applied to the prescribed fire IR imagery. These findings validated that the best approach for our purposes was the fuel moisture-based equation from Smith et al. (2013) (Equation 6). Traditional sampling methods for estimating consumption, while reliable, are often time consuming, not spatially explicit, and less accurate (Lutes et al., 2006; Sikkink & Keane, 2008). This research suggested that UAS-IR imagery may be an alternative option to measuring fuel consumption. Continued in-situ testing of a range of fuel types, moisture contents, and arrangements is needed.

Caution should be exercised when selecting a method to converting fire radiative energy to consumption. Previous research by Hudak et al. (2016) found the energy approach (Equation 4) underestimated consumption, aligning with our results (Figure 3.2). One possible source for the underestimated consumption, from Hudak, was the fuel moisture present. Interestingly, Kremens et al. (2012), where the radiative fraction (*rf*) constant of Equation 4 was developed, did not report any effect from fuel moisture on the energy budget or radiative fraction. Moisture present in fuel is vaporized during the preheating phase of combustion, increasing the latent energy of the energy budget. This in turn reduces the amount of radiative energy emitted by the combusting fuel (Smith et al., 2013). Thus, overlooking the impact fuel moisture has on radiative energy and consumption relationships may lead to underestimation of UAS-predicted consumption. In the context of thermal signal saturation, these results are also limited to the sensor tested because of the relatively low thermal sensor saturation temperature. Without discounting the potential of this particular approach/sensor, it is possible that the plots may have burned at temperatures greater than the saturation point leading to the underestimation of the true FRE.

Pyrometrics derived from UAS imagery proved to be useful for prescribed fire evaluation and monitoring. Three prescribed fires were examined using thermal infrared imagery, yielding spatially explicit measurements of consumption, rate of spread, and residence time. From a qualitative standpoint, these measurements were consistent with visual fire observations, highlighting discernible differences among the burns (Figure 3.5). The semivariograms illustrated that prescribed fire behavior measured at each plot occurs at moderate scales (< 4.6 m). The Nyquist Criterion states that to accurately sample a continuous signal and reconstruct it without aliasing, you must sample at least twice the frequency (or resolution in this context) of the highest frequency component in the signal, suggesting sensor resolutions of less than 2.3 meters are ideal. We sampled fire behavior at sub-meter resolutions, ensuring detailed spatial variability was captured. The Kruskal-Wallis and post-hoc tests of the aggregated pyrometrics illustrated the variability of fire captured but also corroborated that our approach can effectively detect this variability and differentiate between prescribed burn pyrometrics (consumption, rate of spread, and residence time). While the intensities of the prescribed fires sampled were variable, fire effects were characteristic of low severity fire in their respective fire regimes (Fulé et al., 2012; Varner et al., 2005). These sites captured a variety of prescribed fire dynamics in fire tolerant *Pinus* forests, representative of the many scenarios encountered in the US prescribed fire program. Future research could build off this work, testing this process in higher fuel loads and in other forest types.

We found that two out of the three evaluated prescribed fires likely achieved their objectives as far as can be determined from the 2-4 study plots in each fire. However, some of the burns lacked specific objectives related to fuel consumption. Hanna Hammock showcased the fastest rate of spread (peak and average spread) and lowest consumption (Figure 3.5). Given a pre-fire fuel loading of 5.7 Mg ha^{-1} (Table 1) and the consumption objective of 95% fuel reduction (see S3.1 – S3.3 for details on burn objectives), desired consumption was 5.4 Mg ha^{-1}. We estimated consumption averaged 3.0 Mg ha^{-1}, below the desired objective. At this particular burn, adjacent research sampled pre- and post-burn fuel loading data of the site using 25 0.25 m^2 clip-plots (Bigelow et al., 2023). Field fuel sampling inferred consumption to be 3.8 Mg ha^{-1}, or 66% of pre-burn fuel mass. This adjacent study corroborates our consumption estimate and presents solid evidence that the desired outcome of the burn, while stringent, was not achieved. At the Hundred Rx, 50 – 85% reduction in fuel loading was desired, approximately equal to 11 – 22 Mg ha^{-1}. UAS-IR consumption at the two plots sampled was estimated to be 11 and 16 Mg ha^{-1}, so consumption objectives were likely achieved. The Wild Bill Rx burn had significantly higher consumption than any other burn, estimated at 49.2 Mg ha^{-1}. The burn plan only specified post-fire fuel loading (11 – 16 Mg ha^{-1}) and not pre-fire fuel conditions. Given our consumption estimate and the desired post-fire fuel loading specified in the objectives, estimated consumption would equate to 75 – 81%. In similar forest types, desired consumption was specified to be 50 – 85% (Hundred Rx) and 40 – 80% (Waring et al., 2016) reduction in fuel loading. So, it is plausible that the Wild Bill Rx burn achieved consumption objectives, although there remains a degree of uncertainty.

A limitation of our study and the use of aerial infrared sensors was the occlusion of the thermal signal from tree canopy. Canopy foliage intercepted the thermal radiation of the fire, making tree-scale canopy adjustments impossible. While the effect of canopy cover on radiative energy can be modeled at the stand scale (Hudak et al., 2016; Mathews et al., 2016), sub-canopy energy radiation cannot be interpolated at the tree scale given heterogeneous surface fuels. Thus, our approach to monitoring prescribed fire requires unobstructed view of the surface fuels. We suggest our approach only be applied in areas with less than 75% canopy cover, which we adhered to in our study. Future research linking sub-canopy fuel measurements with aerial-IR imagery may be able to mitigate this effect.

Researching prescribed fire during active incidents presented significant challenges. Often, burns were delayed, relocated, and difficult to access. Attending prescribed fires with UAS required extensive authorization from the responsible agency, and Red Card qualified and

FAA Part 107 certified researchers to operate a UAS over an active incident. The prescribed fires attended had a narrow window of favorable weather conditions, so we were usually given 1 – 3 days' notice of location and ignition time. Collecting ground measurements was not possible with the limited time and resources available to us, though these scenarios represent the situations UAS may be implemented in to monitor fire effects. Progressing our knowledge of prescribed fire and application of innovative technologies will require more research on active incidents and active collaboration between practitioners and researchers. Research-led development of software to automatically process UAS-IR imagery collected by fire personnel with UAS qualifications could provide near-instantaneous results of prescribed burn effectiveness so fire and fuel managers could quickly and routinely gather metrics on fires. Data from aerial infrared imagery far surpasses ocular estimates that are currently used and with refinement, can be a powerful tool.

Operationally, our findings support the efficacy of UAS-derived pyrometrics for monitoring and evaluating prescribed fires, specifically consumption, rate of spread, and residence time. Addressing the wildfire crisis will require precise implementation and evaluation of prescribed fire, necessitating a call for robust and precise measurements of objectives. Additionally, we noted that the burn plans of the fires we attended contained broad objectives with wide ranges of desired outcomes. Refined fire monitoring coupled with refined objectives will be pivotal in informing fire management of best practices, justifying the use of prescribed fire, and providing quantitative feedback in an environment saturated with uncertainty. The application of prescribed fire is often subject to constraints due to concerns of disciplinary experts within agencies about the effect of fire on natural and cultural resources. Interdisciplinary cooperation would help prescribed fire to achieve objectives going beyond fuel reduction. For example, detailed UAS-derived pyrometrics could be translated into estimates of belowground heat penetration (heat per unit area and residence time), affecting seed banks and root tissues, as well as aboveground energy release affecting canopy scorch and bole char (O'Brien et al., 2018). Wildlife habitat (Mason & Lashley, 2021) and hydrological impacts (Flerchinger et al., 2016; Williams et al., 2020) can also be linked to fine-scale fire effects. The effect of prescribed burns on cultural resources such as fire-sensitive archeological sites could be monitored in detail, allowing managers to assess whether pre-fire protection efforts such as clearing adjacent fuels were successful (Ryan, 2010).

We found that UAS-derived pyrometrics are an accurate method to estimating consumption and reveal nuanced differences between prescribed fires. Although burn objectives were often broad or not pertaining to fire behavior, we found that consumption objectives were likely achieved for two of the prescribed fires attended. UAS-pyrometrics may serve to inform the next generation of prescribed fire models and provide actionable data for fire management. Extracted data is spatially explicit and high-resolution, suitable for fine-scale prescribed fire research (Hiers et al., 2020). Nonetheless, continued research validating and streamlining the extraction of pyrometrics from UAS is imperative. Work to develop a robust pipeline for processing aerial infrared imagery would be a valuable contribution, especially if the software was open-source and includes a graphical user interface. Additional research is needed to validate infrared-derived pyrometrics and compare their performance against field-sampled equivalent standards, such as residence time and intensity. Prescribed fire behavior is a complex, fine-scale process that is coupled with heterogeneous fuel conditions (Hiers et al., 2020; Hudak et al., 2020). Addressing the wildfire crisis (Singleton et al., 2019; USDA, 2022) will require thoughtful implementation of science-backed treatments followed by detailed monitoring.

5. Acknowledgements

This project wouldn't have been possible without the help of multiple organizations and individuals including Preston Mercer and True Brown from Coconino National Forest; Jeremiah Boyd from Interagency Aviation Management Office; Karen Cummins, Morgan Varner, Seth Bigelow, and Vanessa Niemczyk from Tall Timbers Research Station; Andrew Nordquist from Tonto National Forest; and Floyd Hardin from Salt River Project. This research was funded by National Science Foundation (CPS-2039026) and Salt River Project (Award #8200007407).

Supplemental information

3.S1: Hanna Hammock prescribed fire objectives. From correspondence with Tall Timbers Research Station.

From Eric Staller, Tall Timbers land manager, September 5th, 2023: “My objectives for TT burns are 95% fuel reduction and hardwood top kill. Limbing of pines less than 20 feet tall, and pushing fire deeper to drains and wetlands.”

3.S2: Hundred prescribed fire objectives. From Tonto National Forest 2023 Burn Plan.

> **Resource objectives:** This project is consistent with direction found in the Tonto Land Management Plan for area 5D and 5G. The project area is within Management Area 5D and 5G identified in the Tonto Forest Plan (USDA, 1985, as amended). Management emphasis for this area is to manage for a variety of renewable natural resources with primary emphasis on wildlife habitat, livestock forage and dispersed recreation. Watersheds are managed to meet satisfactory condition. Use prescribed fire to treat vegetation for water yield, forage, and wildlife habitat improvement. The overall intent will be to burn 375 to 15,000 acres per year to reduce the threat of negative impacts to watershed functions including erosion, and reduction in herbaceous productivity.
>
> Project falls within Categorical Exclusion category 32.2 (6) Timber stand and/or wildlife habitat improvement activities that do not include the use of herbicides or do not require more than 1 mile of low standard road construction. (IV). Prescribed burning to reduce natural fuel build-up and improve plant vigor.
>
> **Prescribed fire objectives:** Initial entry burns will use backing fire and strip head fire in ponderosa pine and pinyon/juniper stands to reduce dead and down fuel loadings from 15-20 tons per acre to 10-15 tons per acre. Reduce the under-story vegetation by 75 - 90 percent. Reduce activity slash up to 80 percent. Reduce the over story by no more than 20 percent.
>
> For maintenance burning in ponderosa pine reduce dead and down fuel loadings to 5-7 tons per acre. Reduce the under-story vegetation by 35-90 percent. Reduce the over-story by no more than 15 percent.
>
> In continuous chaparral fuel stands use head fire to reduce the over story density by 50 - 80 percent. Achieve a mosaic burn pattern to create a range of age classes in brush stands. Promote herbaceous species growth by creating openings from 1 - 40 acres in size in accordance with the forest plan.
>
> Objectives should be completed post burn and will be analyzed observationally within the first year.

Desired Effects:

Range of Acceptable Results, Expressed in quantifiable terms:
Ponderosa Pine / Pinyon/Juniper (this will be achieved with first entry and maintenance prescribed burning)

- Reduce Time Lag fuel loadings, 1, 10,100, and 1000 hour by 50% - 85%.
- Reduce under story 35% - 90%.
- Retain a minimum of one snag per acre where applicable.
- Retain 75% - 100% of the desirable trees.

Chaparral Burning

- Reduce over story density by 50% - 80%.
- Create openings of 1 to 200 acres in size with the goal of creating a variety of age class regeneration.
- Achieve a mosaic burn pattern by varied ignition patterns.
- Reduce 1- and 10-hour time lag fuels by 1 - 5 tons per acre.

3.S3: Wild Bill prescribed fire objectives. From Wild Bill incident action plan.

This Burn Plan supports retaining:

- 2 snags per acre, greater than or equal to 30 feet high and 18-inch diameter breast height.
- 3 logs per acre greater than or equal to 12-inch at mid-point.
- 5 to 7 tons of coarse woody debris per acre in the ponderosa pine ecosystem.
- Openings may be up to 4acres with a maximum width of 200'.
- In the pinyon-juniper cover type, snags would be managed for one per acre over 75% of the area and coarse woody debris of 1-3 tons per acre.
- To minimize the potential for crown fire initiation, the desired condition is to have the average stand canopy base height above 18 feet (currently at 16').
- Presently the existing potential for crown fire is 38% through the 4FRI analysis area, and the desired condition is to be at no more than 10%.
- High severity fire should occur on no more than 10% of the treatment area (see below for severity definition).

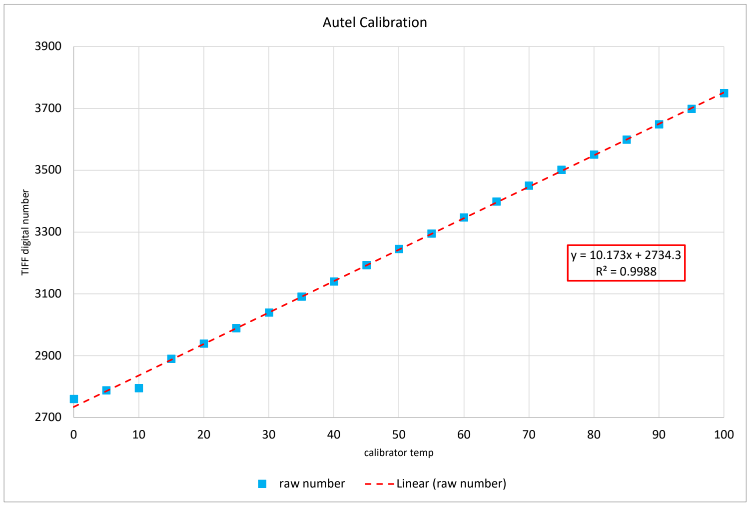

Figure 3.S4: Black body calibration of the LWIR sensor. UAS was positioned ~2 m away from the black body. Temperatures were recorded from the blackbody setting and the average digital number was derived from the UAS IR raster. The maximum temperature of the blackbody was 100 degrees Celsius, so we were unable to assess the performance of the sensor at flaming temperatures.

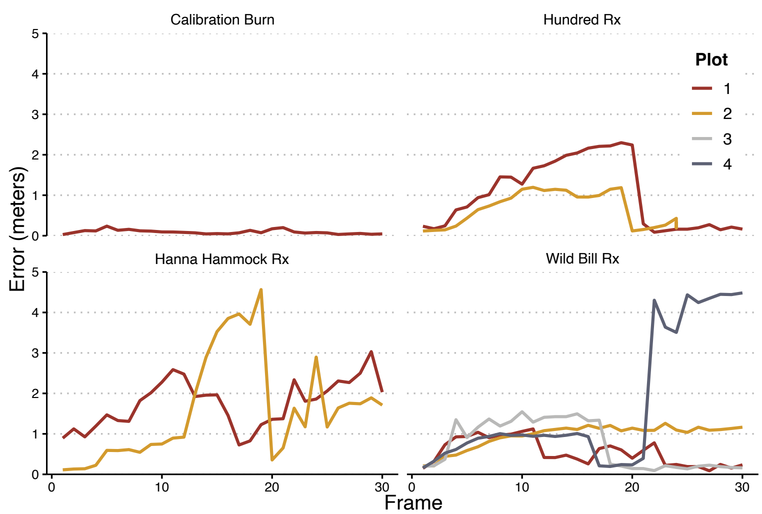

3.S5 Final results stabilization results after georeferencing. While most thermal image stacks had less than two m of positional error relative to the ground control points, instances of significant positional drift is present in some image stacks.

PIXELS, PYROMETRICS, PRESCRIBED FIRE

UAS-INFRARED IMAGERY AS AN ACCURATE FIRE MONITORING TOOL

Introduction

The “Wildfire crisis” is upon us, and making science-informed, proactive decisions is crucial for the sustainability and restoration of forested landscapes. Prescribed fire is one treatment option that can significantly reduce fire hazard while reintroducing a natural disturbance mechanism to fire-adapted ecosystems.

Prescribed fire is a planned treatment that demands clear objectives and measurable benefits. Monitoring efforts should be designed to inform fire management and encourage the use of prescribed burning as an effective treatment practice. Research using innovative tools for fire management will improve our **knowledge, effectiveness, and application** of using prescribed fire.

We used infrared imagery collected from prescribed fires to quantify fire behavior and evaluate the fire in meeting objectives (Fig. 1). To do this we, developed a process where we ‘parked’ the uncrewed aircraft system (UAS) ~400’ above ground over the fire, taking images of the burn every 5 seconds for the duration of the burn. Then, we stabilized and calibrated the images, and generated **pyrometrics: detailed measurements of fire behavior such as consumption, rate of spread, and residence time of the fire** (Fig. 2). Additionally, we validated our consumption methods by comparing UAS-estimated consumption with weight-based consumption.

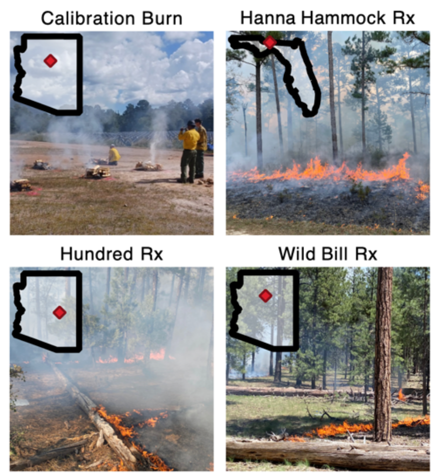

Figure 1: Locations and images of fire behavior of each of the prescribed burns and the calibration burn.

Results

Our consumption estimates using the UAS were notably accurate, validating our approach to convert energy to fuel consumed. Our UAS-fire metrics of three prescribed fires supported visually observed estimates of fire behavior: Hanna Hammock Rx was notably much faster spreading (45 chains/hr) than the Arizona burns (12 chains/hr) and Wild Bill Rx had the highest consumption (22 t/ac).

Comparing our findings with the burn objectives, two of the three prescribed fires likely achieved desired consumption goals. We also noted that the objectives for some of the burns were broad in scope, did not specify consumption, and had a wide range of desired conditions.

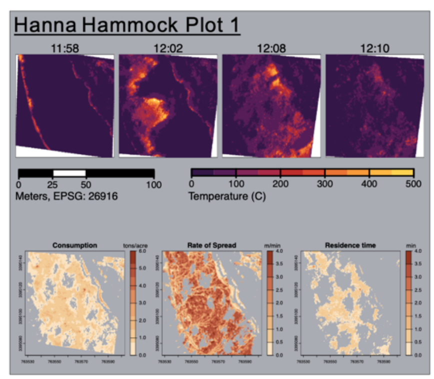

Figure 2: Selection of the infrared imagery from Hanna Hammock prescribed fire and the derived pyrometrics: consumption, rate of spread, and residence time.

FACT SHEET CONTINUED: PIXELS, PYROMETRICS, PRESCRIBED FIRE

Management implications

Evaluation: using UAS and this processing approach, managers can determine if prescribed fires are meeting objectives.

Feedback: Inform managers of "cause and effect" of how burning in different fuel types, weather conditions, firing patterns can change the outcome of the burn.

Efficient: UAS are cost-effective and have the potential to be automated, so fire monitoring does not commit personnel and resources during demanding situations.

Spatially Explicit: UAS-data is spatially explicit (unlike traditional monitoring methods), so fine-scale patterns of prescribed fire can be quantified. This is critical our ecological understanding of fire refugia and how fire mosaics affect understory diversity.

Justification: With precise monitoring supporting that objective achievement, managers can justify the use of prescribed fire as an effective fuels treatment.

Validation: UAS pyrometrics can validate fire and fuel models, improving performance and application

IN A NUTSHELL:

- Prescribed fire is a treatment that necessitates monitoring and evaluation
- We developed a workflow to monitor prescribed fires with uncrewed aircraft systems (UAS), accurately estimating consumption
- Our research can be applied to inform fire managers of fire outcomes, study fine-scale fire dynamics, justify the use of prescribed fire, and validate new computational fire models.

REFERENCES

Abatzoglou, J. T., & Williams, A. P. (2016). Impact of anthropogenic climate change on wildfire across western US forests. *Proceedings of the National Academy of Sciences*, *113*(42), 11770–11775. https://doi.org/10.1073/pnas.1607171113

Agisoft. (2023). *Metashape Professional* (2.0). Agisoft. https://www.agisoft.com/

Ahamed, A., Foye, J., Poudel, S., Trieschman, E., & Fike, J. (2023). Measuring tree diameter with photogrammetry using mobile phone cameras. *Forests*, *14*(10), 2027. https://doi.org/10.3390/f14102027

Alcantarilla, P. F., Bartoli, A., & Davison, A. J. (2012). KAZE Features. *Computer Vision*, *7577 LNCS*, 214–227. https://doi.org/10.1007/978-3-642-33783-3_16

Bekar, A., Antoniou, M., & Baker, C. J. (2021). High-resolution drone-borne SAR using off-the-shelf high-frequency radars. *IEEE National Radar Conference - Proceedings*, *2021-May*. https://doi.org/10.1109/RadarConf2147009.2021.9455342

Belmonte, A., Sankey, T., Biederman, J. A., Bradford, J., Goetz, S. J., Kolb, T., & Woolley, T. (2020). UAV-derived estimates of forest structure to inform ponderosa pine forest restoration. *Remote Sensing in Ecology and Conservation*, *6*(2), 181–197. https://doi.org/10.1002/rse2.137

Bienert, A., Hess, C., Maas, H.-G., & von Oheimb, G. (2014). A voxel-based technique to estimate the volume of trees from terrestrial laser scanner data. *The International Archives of the Photogrammetry, Remote Sensing and Spatial Information Sciences*, *XL–5*(5), 101–106. https://doi.org/10.5194/isprsarchives-XL-5-101-2014

Bigelow, S. W., Niemcyzk, V., & Hoynes, K. (2023). *Data collection for Hanna Hammock Prescribed Burn*.

Bond, W. J., & Keeley, J. E. (2005). Fire as a global 'herbivore': the ecology and evolution of flammable ecosystems. *Trends in Ecology & Evolution*, *20*(7), 387–394. https://doi.org/10.1016/J.TREE.2005.04.025

Bowman, D. M. J. S., Balch, J. K., Artaxo, P., Bond, W. J., Carlson, J. M., Cochrane, M. A., D'Antonio, C. M., DeFries, R. S., Doyle, J. C., Harrison, S. P., Johnston, F. H., Keeley, J. E., Krawchuk, M. A., Kull, C. A., Marston, J. B., Moritz, M. A., Prentice, I. C., Roos, C. I., Scott, A. C., … Pyne, S. J. (2009). Fire in the Earth System. *Science*, *324*(5926), 481–484. https://doi.org/10.1126/science.1163886

Bradski, G. (2000). *The OpenCV Library*. Dr. Dobb's Journal of Software Tools.

Brede, B., Calders, K., Lau, A., Raumonen, P., Bartholomeus, H. M., Herold, M., & Kooistra, L. (2019). Non-destructive tree volume estimation through quantitative structure modelling: Comparing UAV laser scanning with terrestrial LIDAR. *Remote Sensing of Environment*, *233*, 111355. https://doi.org/10.1016/j.rse.2019.111355

Bright, B. C., Hudak, A. T., McCarley, T. R., Spannuth, A., Sánchez-López, N., Ottmar, R. D., & Soja, A. J. (2022). Multitemporal lidar captures heterogeneity in fuel loads and consumption on the Kaibab Plateau. *Fire Ecology*, *18*(1), 1–16. https://doi.org/10.1186/s42408-022-00142-7

Calders, K., Adams, J., Armston, J., Bartholomeus, H., Bauwens, S., Bentley, L. P., Chave, J., Danson, F. M., Demol, M., Disney, M., Gaulton, R., Krishna Moorthy, S. M., Levick, S. R., Saarinen, N., Schaaf, C., Stovall, A., Terryn, L., Wilkes, P., & Verbeeck, H. (2020). Terrestrial laser scanning in forest ecology: Expanding the horizon. *Remote Sensing of Environment*, *251*, 112102. https://doi.org/10.1016/J.RSE.2020.112102

Calders, K., Newnham, G., Burt, A., Murphy, S., Raumonen, P., Herold, M., Culvenor, D., Avitabile, V., Disney, M., Armston, J., & Kaasalainen, M. (2015). Nondestructive estimates of above-ground biomass using terrestrial laser scanning. *Methods in Ecology and Evolution*, *6*(2), 198–208. https://doi.org/10.1111/2041-210X.12301

Calders, K., Verbeeck, H., Burt, A., Origo, N., Nightingale, J., Malhi, Y., Wilkes, P., Raumonen, P., Bunce, R. G. H., & Disney, M. (2022). Laser scanning reveals potential underestimation of biomass carbon in temperate forest. *Ecological Solutions and Evidence*, *3*(4), e12197. https://doi.org/10.1002/2688-8319.12197

Cansler, C. A., Kane, V. R., Hessburg, P. F., Kane, J. T., Jeronimo, S. M. A., Lutz, J. A., Povak, N. A., Churchill, D. J., & Larson, A. J. (2022). Previous wildfires and management treatments moderate subsequent fire severity. *Forest Ecology and Management*, *504*, 119764. https://doi.org/10.1016/j.foreco.2021.119764

Chamberlain, C. P., Sánchez Meador, A. J., & Thode, A. E. (2021). Airborne lidar provides reliable estimates of canopy base height and canopy bulk density in southwestern ponderosa pine forests. *Forest Ecology and Management*, *481*, 118695. https://doi.org/10.1016/j.foreco.2020.118695

Chen, X., Hopkins, B., Wang, H., O'Neill, L., Afghah, F., Razi, A., Fulé, P., Coen, J., Rowell, E., & Watts, A. (2022). Wildland fire detection and monitoring using a drone-collected RGB/IR image dataset. *IEEE Access*, *10*, 121301–121317. https://doi.org/10.1109/ACCESS.2022.3222805

Cook, K. L. (2017). An evaluation of the effectiveness of low-cost UAVs and structure from motion for geomorphic change detection. *Geomorphology*, *278*, 195–208. https://doi.org/10.1016/J.GEOMORPH.2016.11.009

de Almeida, D. R. A., Stark, S. C., Valbuena, R., Broadbent, E. N., Silva, T. S. F., de Resende, A. F., Ferreira, M. P., Cardil, A., Silva, C. A., Amazonas, N., Zambrano, A. M. A., & Brancalion, P. H. S. (2020). A new era in forest restoration monitoring. *Restoration Ecology*, *28*(1), 8–11. https://doi.org/10.1111/REC.13067

Dickinson, M. B., Hudak, A. T., Zajkowski, T., Loudermilk, E. L., Schroeder, W., Ellison, L., Kremens, R. L., Holley, W., Martinez, O., Paxton, A., Bright, B. C., O'Brien, J. J., Hornsby, B., Ichoku, C., Faulring, J., Gerace, A., Peterson, D., & Mauceri, J. (2016). Measuring radiant emissions from entire prescribed fires with ground, airborne and satellite sensors - RxCADRE 2012. *International Journal of Wildland Fire*, *25*(1), 48–61. https://doi.org/10.1071/WF15090

Donager, J. J., Sánchez Meador, A. J., & Blackburn, R. C. (2021). Adjudicating perspectives on forest structure: How do airborne, terrestrial, and mobile lidar-derived estimates compare? *Remote Sensing*, *13*(12), 2297. https://doi.org/10.3390/rs13122297

Donager, J. J., Sankey, T. T., Sankey, J. B., Sanchez Meador, A. J., Springer, A. E., & Bailey, J. D. (2018). Examining forest structure with terrestrial lidar: Suggestions and novel techniques based on comparisons between scanners and forest treatments. *Earth and Space Science*, *5*(11), 753–776. https://doi.org/10.1029/2018EA000417

Evangelidis, G. D., & Psarakis, E. Z. (2008). Parametric image alignment using enhanced correlation coefficient maximization. *IEEE Transactions on Pattern Analysis and Machine Intelligence*, *30*(10), 1858–1865. https://doi.org/10.1109/TPAMI.2008.113

Fernandes, P. M., & Botelho, H. S. (2003). A review of prescribed burning effectiveness in fire hazard reduction. *International Journal of Wildland Fire*, *12*(2), 117. https://doi.org/10.1071/WF02042

Fernández-Guisuraga, J. M., Suárez-Seoane, S., Fernandes, P. M., Fernández-García, V., Fernández-Manso, A., Quintano, C., & Calvo, L. (2022). Pre-fire aboveground biomass, estimated from LiDAR, spectral and field inventory data, as a major driver of burn severity in maritime pine (Pinus pinaster) ecosystems. *Forest Ecosystems*, *9*, 100022. https://doi.org/10.1016/J.FECS.2022.100022

Filkov, A., Cirulis, B., & Penman, T. (2021). Quantifying merging fire behaviour phenomena using unmanned aerial vehicle technology. *International Journal of Wildland Fire*, *30*(3), 197–214. https://doi.org/10.1071/WF20088

Flerchinger, G. N., Seyfried, M. S., & Hardegree, S. P. (2016). Hydrologic response and recovery to prescribed fire and vegetation removal in a small rangeland catchment. *Ecohydrology*, *9*(8), 1604–1619. https://doi.org/10.1002/eco.1751

Freeborn, P. H., Wooster, M. J., Hao, W. M., Ryan, C. A., Nordgren, B. L., Baker, S. P., & Ichoku, C. (2008). Relationships between energy release, fuel mass loss, and trace gas and aerosol emissions during laboratory biomass fires. *Journal of Geophysical Research: Atmospheres*, *113*(D1), 1301. https://doi.org/10.1029/2007JD008679

Fulé, P. Z., Covington, W. W., & Moore, M. M. (1997). Determining reference conditions for ecosystem management of southwestern ponderosa pine forests. *Ecological Applications*, *7*(3), 895–908. https://doi.org/10.1890/1051-0761(1997)007[0895:DRCFEM]2.0.CO;2

Fulé, P. Z., Crouse, J. E., Roccaforte, J. P., & Kalies, E. L. (2012). Do thinning and/or burning treatments in western USA ponderosa or Jeffrey pine-dominated forests help restore natural fire behavior? *Forest Ecology and Management*, *269*, 68–81. https://doi.org/10.1016/J.FORECO.2011.12.025

GDAL/OGR Contributors. (2023). *GDAL/OGR Geospatial Data Abstraction software Library* (3). Open Source Geospatial Foundation. https://doi.org/10.5281/zenodo.5884351

Gowravaram, S., Chao, H., Zhao, T., Parsons, S., Hu, X., Xin, M., Flanagan, H., & Tian, P. (2022). Prescribed grass fire evolution mapping and rate of spread measurement using orthorectified thermal imagery from a fixed-wing UAS. *International Journal of Remote Sensing*, *43*(7), 2357–2376. https://doi.org/10.1080/01431161.2022.2044538

Hartley, R. J. L., Davidson, S. J., Watt, M. S., Massam, P. D., Aguilar-Arguello, S., Melnik, K. O., Pearce, H. G., & Clifford, V. R. (2022). A Mixed Methods Approach for Fuel Characterisation in Gorse (Ulex europaeus L.) Scrub from High-Density UAV Laser Scanning Point Clouds and Semantic Segmentation of UAV Imagery. *Remote Sensing*, *14*(19), 4775. https://doi.org/10.3390/rs14194775

Hengl, T. (2006). Finding the right pixel size. *Computers & Geosciences*, *32*(9), 1283–1298. https://doi.org/10.1016/j.cageo.2005.11.008

Hessburg, P. F., Miller, C. L., Parks, S. A., Povak, N. A., Taylor, A. H., Higuera, P. E., Prichard, S. J., North, M. P., Collins, B. M., Hurteau, M. D., Larson, A. J., Allen, C. D., Stephens, S. L., Rivera-Huerta, H., Stevens-Rumann, C. S., Daniels, L. D., Gedalof, Z., Gray, R. W., Kane, V. R., … Salter, R. B. (2019). Climate, Environment, and Disturbance History Govern Resilience of Western North American Forests. *Frontiers in Ecology and Evolution*, *7*, 445132. https://doi.org/10.3389/FEVO.2019.00239/BIBTEX

Hiers, J. K., Jackson, S. T., Hobbs, R. J., Bernhardt, E. S., & Valentine, L. E. (2016). The Precision Problem in Conservation and Restoration. *Trends in Ecology & Evolution*, *31*(11), 820–830. https://doi.org/10.1016/J.TREE.2016.08.001

Hiers, J. K., O'Brien, J. J., Varner, J. M., Butler, B. W., Dickinson, M., Furman, J., Gallagher, M., Godwin, D., Goodrick, S. L., Hood, S. M., Hudak, A., Kobziar, L. N., Linn, R., Loudermilk, E. L., McCaffrey, S., Robertson, K., Rowell, E. M., Skowronski, N., Watts, A. C., & Yedinak, K. M. (2020). Prescribed fire science: the case for a refined research agenda. *Fire Ecology*, *16*(1), 11. https://doi.org/10.1186/s42408-020-0070-8

Hillman, S., Hally, B., Wallace, L., Turner, D., Lucieer, A., Reinke, K., & Jones, S. (2021). High-resolution estimates of fire severity—an evaluation of uas image and lidar mapping approaches on a sedgeland forest boundary in Tasmania, Australia. *Fire*, *4*(1), 14. https://doi.org/10.3390/fire4010014

Hoffman, C. M., Sieg, C. H., Linn, R. R., Mell, W., Parsons, R. A., Ziegler, J. P., & Hiers, J. K. (2018). Advancing the science of wildland fire dynamics using process-based models. *Fire*, *1*(2), 1–6. https://doi.org/10.3390/fire1020032

Hudak, A. T., Dickinson B, M. B., Bright, B. C., Kremens, R. L., Loudermilk, E. L., O'brien, J. J., Hornsby, B. S., & Ottmar, R. D. (2016). Measurements relating fire radiative energy density and surface fuel consumption - RxCADRE 2011 and 2012. *International Journal of Wildland Fire*, *25*. https://doi.org/10.1071/WF14159

Hudak, A. T., Freeborn, P. H., Lewis, S. A., Hood, S. M., Smith, H. Y., Hardy, C. C., Kremens, R. J., Butler, B. W., Teske, C., Tissell, R. G., Queen, L. P., Nordgren, B. L., Bright, B. C., Morgan, P., Riggan, P. J., Macholz, L., Lentile, L. B., Riddering, J. P., & Mathews, E. E. (2018). The cooney ridge fire experiment: An early operation to relate pre-, active, and post-fire field and remotely sensed measurements. *Fire*, *1*(1), 1–32. https://doi.org/10.3390/fire1010010

Hudak, A. T., Kato, A., Bright, B. C., Loudermilk, E. L., Hawley, C., Restaino, J. C., Ottmar, R. D., Prata, G. A., Cabo, C., Prichard, S. J., Rowell, E. M., & Weise, D. R. (2020). Towards spatially explicit quantification of pre-and postfire fuels and fuel consumption from traditional and point cloud measurements. *Forest Science*, *66*(4), 428–442. https://doi.org/10.1093/forsci/fxz085

Hurteau, M. D., Bradford, J. B., Fulé, P. Z., Taylor, A. H., & Martin, K. L. (2014). Climate change, fire management, and ecological services in the southwestern US. *Forest Ecology and Management*, *327*, 280–289. https://doi.org/10.1016/J.FORECO.2013.08.007

Hyyppä, E., Yu, X., Kaartinen, H., Hakala, T., Kukko, A., Vastaranta, M., & Hyyppä, J. (2020). Comparison of backpack, handheld, under-canopy UAV, and above-canopy UAV laser scanning for field reference data collection in boreal forests. *Remote Sensing*, *12*(20), 1–31. https://doi.org/10.3390/rs12203327

Hyyppä, J., & Inkinen, M. (1999). Detecting and estimating attributes for single trees using laser scanner. *The Photogrammetric Journal of Finnland*, *16*(2).

Iglhaut, J., Cabo, C., Puliti, S., Piermattei, L., O'Connor, J., & Rosette, J. (2019). Structure from Motion photogrammetry in forestry: a review. *Current Forestry Reports*, *5*(3), 155–168. https://doi.org/10.1007/s40725-019-00094-3

Iverson, L. R., Yaussy, D. A., Rebbeck, J., Hutchinson, T. F., Long, R. P., & Prasad, A. M. (2004). A comparison of thermocouples and temperature paints to monitor spatial and temporal characteristics of landscape-scale prescribed fires. *International Journal of Wildland Fire*, *13*(3), 311–322. https://doi.org/10.1071/WF03063

Jain, P., Coogan, S. C., Ganapathi Subramanian, S., Crowley, M., Taylor, S., Flannigan, M. D., Coogan, S., Subramanian, S., Crowley, M., & Taylor, S. (2020). A review of machine learning applications in wildfire science and management. *Environmental Reviews*, *28*, 478–505. https://doi.org/10.1139/er-2020-0019

Johnston, J. M., Wheatley, M. J., Wooster, M. J., Paugam, R., Matt Davies, G., & Deboer, K. A. (2018). Flame-front rate of spread estimates for moderate scale experimental fires are strongly influenced by measurement approach. *Fire*, *1*(1), 1–17. https://doi.org/10.3390/fire1010016

Johnston, J. M., Wooster, M. J., & Lynham, T. J. (2014). Experimental confirmation of the MWIR and LWIR grey body assumption for vegetation fire flame emissivity. *International Journal of Wildland Fire*, *23*(4), 463–479. https://doi.org/10.1071/WF12197

Kennard, D. K., Outcalt, K. W., Jones, D., & O'Brien, J. J. (2005). Comparing Techniques for Estimating Flame Temperature of Prescribed Fires. *Fire Ecology 2005 1:1*, *1*(1), 75–84. https://doi.org/10.4996/FIREECOLOGY.0101075

Kremens, R. L., Dickinson, M. B., & Bova, A. S. (2012). Radiant flux density, energy density and fuel consumption in mixed-oak forest surface fires. *International Journal of Wildland Fire*, *21*(6), 722–730. https://doi.org/10.1071/WF10143

Krisanski, S., Perugia, B. Del, Taskhiri, M. S., & Turner, P. (2018). Below-canopy UAS photogrammetry for stem measurement in radiata pine plantation. *Remote Sensing*, *10783*, 45–55. https://doi.org/10.1117/12.2325480

Krisanski, S., Taskhiri, M. S., Gonzalez Aracil, S., Herries, D., Muneri, A., Gurung, M. B., Montgomery, J., & Turner, P. (2021). Forest Structural Complexity Tool—An Open Source, Fully-Automated Tool for Measuring Forest Point Clouds. *Remote Sensing*, *13*(22), 4677. https://doi.org/10.3390/rs13224677

Krisanski, S., Taskhiri, M. S., & Turner, P. (2020). Enhancing methods for under-canopy unmanned aircraft system based photogrammetry in complex forests for tree diameter measurement. *Remote Sensing*, *12*(10), 1652. https://doi.org/10.3390/rs12101652

Levoy, M., & Whitted, T. (1985). *The Use of Points as a Display Primitive*. 1–16. https://citeseerx.ist.psu.edu/document?repid=rep1&type=pdf&doi=3a6aa5ef72eeef9543695b3cc70f72576fc1651f

Lim, K., Treitz, P., Wulder, M., St-Onge, B., & Flood, M. (2003). LiDAR remote sensing of forest structure. *Progress in Physical Geography: Earth and Environment*, *27*(1), 88–106. https://doi.org/10.1191/0309133303pp360ra

López, A., Molina-Aiz, F. D., Valera, D. L., & Peña, A. (2012). Determining the emissivity of the leaves of nine horticultural crops by means of infrared thermography. *Scientia Horticulturae*, *137*, 49–58. https://doi.org/10.1016/j.scienta.2012.01.022

Loudermilk, E. L., O'Brien, J. J., Mitchell, R. J., Cropper, W. P., Hiers, J. K., Grunwald, S., Grego, J., & Fernandez-Diaz, J. C. (2012). Linking complex forest fuel structure and fire behaviour at fine scales. *International Journal of Wildland Fire*, *21*(7), 882. https://doi.org/10.1071/WF10116

Lowe, D. G. (1999). Object recognition from local scale-invariant features. *Proceedings of the IEEE International Conference on Computer Vision*, *2*, 1150–1157. https://doi.org/10.1109/ICCV.1999.790410

Lutes, D. C., Keane, R. E., Caratti, J. F., Key, C. H., Benson, N. C., Sutherland, S., & Gangi, L. J. (2006). FIREMON: Fire effects monitoring and inventory system. *Gen. Tech. Rep. RMRS-GTR-164*, *164*. https://doi.org/10.2737/RMRS-GTR-164

Mahesh, & Subramanyam, M. V. (2012). Automatic feature based image registration using SIFT algorithm. *2012 Third International Conference on Computing, Communication and Networking Technologies (ICCCNT'12)*, 1–5. https://doi.org/10.1109/ICCCNT.2012.6396024

Maltamo, M., Næsset, E., & Vauhkonen, J. (2014). *Forestry Applications of Airborne Laser Scanning* (Vol. 27). Springer Netherlands. https://doi.org/10.1007/978-94-017-8663-8

Manfreda, S., McCabe, M. F., Miller, P. E., Lucas, R., Madrigal, V. P., Mallinis, G., Dor, E. Ben, Helman, D., Estes, L., Ciraolo, G., Müllerová, J., Tauro, F., de Lima, M. I., de Lima, J. L. M. P., Maltese, A., Frances, F., Caylor, K., Kohv, M., Perks, M., … Toth, B. (2018). On the use of unmanned aerial systems for environmental monitoring. In *Remote Sensing* (Vol. 10, Issue 4, p. 641). Multidisciplinary Digital Publishing Institute. https://doi.org/10.3390/rs10040641

Martin, R., Cushwa, C., & Miller, R. (1969). Fire as a physical factor in wildland management. *Proceedings of the Ninth Annual Tall Timbers Fire Ecology Conference*, 271–288.

Mason, D. S., & Lashley, M. A. (2021). Spatial scale in prescribed fire regimes: an understudied aspect in conservation with examples from the southeastern United States. *Fire Ecology 2021 17:1*, *17*(1), 1–14. https://doi.org/10.1186/S42408-020-00087-9

Mathews, B. J., Strand, E. K., Smith, A. M. S., Hudak, A. T., Dickinson, B., & Kremens, R. L. (2016). Laboratory experiments to estimate interception of infrared radiation by tree canopies. *International Journal of Wildland Fire*, *25*(9), 1009–1014. https://doi.org/10.1071/WF16007

Moore, B., Thompson, D. K., Schroeder, D., Johnston, J. M., & Hvenegaard, S. (2020). Using infrared imagery to assess fire behaviour in a mulched fuel bed in black spruce forests. *Fire*, *3*(3), 1–11. https://doi.org/10.3390/fire3030037

Moran, C. J., Hoff, V., Parsons, R. A., Queen, L. P., & Seielstad, C. A. (2022). Mapping Fine-Scale Crown Scorch in 3D with Remotely Piloted Aircraft Systems. *Fire*, *5*(3), 59. https://doi.org/10.3390/fire5030059

Moran, C. J., Kane, V. R., & Seielstad, C. A. (2020). Mapping forest canopy fuels in the western united states with LiDAR-Landsat covariance. *Remote Sensing*, *12*(6), 1000. https://doi.org/10.3390/rs12061000

Moran, C. J., Seielstad, C. A., Cunningham, M. R., Hoff, V., Parsons, R. A., Queen, L., Sauerbrey, K., & Wallace, T. (2019). Deriving fire behavior metrics from UAS imagery. *Fire*, *2*(2), 1–20. https://doi.org/10.3390/fire2020036

Nelson, R., Krabill, W., & MacLean, G. (1984). Determining forest canopy characteristics using airborne laser data. *Remote Sensing of Environment*, *15*(3), 201–212. https://doi.org/10.1016/0034-4257(84)90031-2

Nitoslawski, S. A., Wong-Stevens, K., Steenberg, J. W. N., Witherspoon, K., Nesbitt, L., & Konijnendijk van den Bosch, C. C. (2021). The digital forest: Mapping a decade of knowledge on technological applications for forest ecosystems. *Earth's Future*, *9*(8), e2021EF002123. https://doi.org/10.1029/2021EF002123

O'Brien, J. J., Hiers, J. K., Varner, J. M., Hoffman, C. M., Dickinson, M. B., Michaletz, S. T., Loudermilk, E. L., & Butler, B. W. (2018). Advances in mechanistic approaches to quantifying biophysical fire effects. *Current Forestry Reports*, *4*(4), 161–177. https://doi.org/10.1007/s40725-018-0082-7

O'Brien, J. J., Loudermilk, E. L., Hornsby, B., Hudak, A. T., Bright, B. C., Dickinson, M. B., Hiers, J. K., Teske, C., Ottmar, R. D., O'Brien, J. J., Loudermilk, E. L., Hornsby, B., Hudak, A. T., Bright, B. C., Dickinson, M. B., Hiers, J. K., Teske, C., & Ottmar, R. D. (2015). High-resolution infrared thermography for capturing wildland fire behaviour: RxCADRE 2012. *International Journal of Wildland Fire*, *25*(1), 62–75. https://doi.org/10.1071/WF14165

Packalen, P., Strunk, J., Packalen, T., Maltamo, M., & Mehtätalo, L. (2019). Resolution dependence in an area-based approach to forest inventory with airborne laser scanning. *Remote Sensing of Environment*, *224*, 192–201. https://doi.org/10.1016/J.RSE.2019.01.022

Parsons, R. A., Linn, R. R., Pimont, F., Hoffman, C., Sauer, J., Winterkamp, J., Sieg, C. H., & Jolly, W. M. (2017). Numerical Investigation of Aggregated Fuel Spatial Pattern Impacts on Fire Behavior. *Land 2017, Vol. 6, Page 43*, *6*(2), 43. https://doi.org/10.3390/LAND6020043

Parsons, R. A., Wells, L., Marcozzi, A., Linn, R., Hiers, K., Pimont, F., Riley, K., Altintas, I., & Flanary, S. (2023). Going 3D With Fuel and Fire Modeling: FastFuels and QUIC-Fire. *Fire Management Today*, *81*(1), 48–51. https://www.fs.usda.gov/sites/default/files/fire-management-today/fmt-vol-81-n1.pdf

Paugam, R., Wooster, M. J., Mell, W. E., Rochoux, M. C., Filippi, J.-B., Rücker, G., Frauenberger, O., Lorenz, E., Schroeder, W., Main, B., & Govender, N. (2021). Orthorectification of Helicopter-Borne High Resolution Experimental Burn Observation from Infra Red Handheld Imagers. *Remote Sensing*, *13*(23), 4913. https://doi.org/10.3390/rs13234913

Paugam, R., Wooster, M. J., & Roberts, G. (2013). Use of handheld thermal imager data for airborne mapping of fire radiative power and energy and flame front rate of spread. *IEEE Transactions on Geoscience and Remote Sensing*, *51*(6), 3385–3399. https://doi.org/10.1109/TGRS.2012.2220368

Perrakis, D. D. B., Cruz, M. G., Alexander, M. E., Taylor, S. W., & Beverly, J. L. (2019). Linking dynamic empirical fire spread models: introducing Canadian Conifer Pyrometrics. *Proceedings of 6th Fuels and Fire Behavior Conference*, 67–72. https://www.frames.gov/catalog/62104

Prichard, S. J., Hessburg, P. F., Hagmann, R. K., Povak, N. A., Dobrowski, S. Z., Hurteau, M. D., Kane, V. R., Keane, R. E., Kobziar, L. N., Kolden, C. A., North, M., Parks, S. A., Safford, H. D., Stevens, J. T., Yocom, L. L., Churchill, D. J., Gray, R. W., Huffman, D. W., Lake, F. K., & Khatri-Chhetri, P. (2021). Adapting western North American forests to climate change and wildfires: 10 common questions. *Ecological Applications*, *31*(8), e02433. https://doi.org/10.1002/EAP.2433

Reeves, M. C., Ryan, K. C., Rollins, M. G., & Thompson, T. G. (2009). Spatial fuel data products of the LANDFIRE Project. *International Journal of Wildland Fire*, *18*, 250–267. https://doi.org/10.1071/WF08086

Reid, A. M., & Robertson, K. M. (2012). Energy content of common fuels in upland pine savannas of the south-eastern US and their application to fire behaviour modelling. *International Journal of Wildland Fire*, *21*(5), 591. https://doi.org/10.1071/WF10139

Reilly, S., Clark, M. L., Bentley, L. P., Matley, C., Piazza, E., & Oliveras Menor, I. (2021). The potential of multispectral imagery and 3d point clouds from unoccupied aerial systems (Uas) for monitoring forest structure and the impacts of wildfire in mediterranean-climate forests. *Remote Sensing*, *13*(19), 3810. https://doi.org/10.3390/rs13193810

Reynolds, R. T., Sánchez Meador, A. J., Youtz, J. A., Nicolet, T., Matonis, M. S., Jackson, P. L., DeLorenzo, D. G., & Graves, A. D. (2013). Restoring composition and structure in southwestern firequent-fire forests: A science-based framework for improving ecosystem resiliency. In *General Technichal Report RMRS-GTR-310*. https://www.fs.usda.gov/rm/pubs/rmrs_gtr310.pdf

Roccaforte, J. P., Fulé, P. Z., Chancellor, W. W., & Laughlin, D. C. (2012). Woody debris and tree regeneration dynamics following severe wildfires in Arizona ponderosa pine forests. *Canadian Journal of Forest Research*, *42*(3), 593–604. https://doi.org/10.1139/x2012-010

Rothermel, R. C., & Deeming, J. E. (1980). Measuring and interpreting fire behavior for correlation with fire effects. *General Technical Report INT-93*.

Rowell, E., Loudermilk, E. L., Hawley, C., Pokswinski, S., Seielstad, C., Queen, Ll., O'Brien, J. J., Hudak, A. T., Goodrick, S., & Hiers, J. K. (2020). Coupling terrestrial laser scanning with 3D fuel biomass sampling for advancing wildland fuels characterization. *Forest Ecology and Management*, *462*, 117945. https://doi.org/10.1016/j.foreco.2020.117945

Ryan, K. C. (2010). Effects of fire on cultural resources. In D. Viegas (Ed.), *VI International Conference on Forest Fire Research*. Rocky Mountain Research Station. https://www.fs.usda.gov/rm/pubs_other/rmrs_2010_ryan_k004.pdf

Ryan, K. C., Knapp, E. E., & Varner, J. M. (2013). Prescribed fire in North American forests and woodlands: history, current practice, and challenges. *Frontiers in Ecology and the Environment*, *11*(s1), e15–e24. https://doi.org/10.1890/120329

Sagel, D., Speer, K., Pokswinski, S., & Quaife, B. (2021). Fine-scale fire spread in pine straw. *Fire*, *4*(4), 69. https://doi.org/10.3390/fire4040069

Schumacher, B., Melnik, K. O., Katurji, M., Zhang, J., Clifford, V., Pearce, H. G., Schumacher, B., Melnik, K. O., Katurji, M., Zhang, J., Clifford, V., & Pearce, H. G. (2022). Rate of spread and flaming zone velocities of surface fires from visible and thermal image processing. *International Journal of Wildland Fire*, *31*(8), 759–773. https://doi.org/10.1071/WF21122

Shamsoshoara, A., Afghah, F., Razi, A., Zheng, L., Fulé, P. Z., & Blasch, E. (2021). Aerial imagery pile burn detection using deep learning: The FLAME dataset. *Computer Networks*, *193*, 108001. https://doi.org/10.1016/J.COMNET.2021.108001

Shannon, C. E. (1949). Communication in the Presence of Noise. *Proceedings of the IRE*, *37*(1), 10–21. https://doi.org/10.1109/JRPROC.1949.232969

Shin, P., Sankey, T., Moore, M. M., & Thode, A. E. (2018). Evaluating unmanned aerial vehicle images for estimating forest canopy fuels in a ponderosa pine stand. *Remote Sensing*, *10*(8), 1266. https://doi.org/10.3390/rs10081266

Sikkink, P. G., & Keane, R. E. (2008). A comparison of five sampling techniques to estimate surface fuel loading in montane forests. *International Journal of Wildland Fire*, *17*(3), 363–379. https://doi.org/10.1071/WF07003

Singleton, M. P., Thode, A. E., Sánchez Meador, A. J., & Iniguez, J. M. (2019). Increasing trends in high-severity fire in the southwestern USA from 1984 to 2015. *Forest Ecology and Management*, *433*, 709–719. https://doi.org/10.1016/j.foreco.2018.11.039

Skowronski, N. S., Gallagher, M. R., & Warner, T. A. (2020). Decomposing the interactions between fire severity and canopy fuel structure using multi-temporal, active, and passive remote sensing approaches. *Fire*, *3*(1), 1–21. https://doi.org/10.3390/fire3010007

Smith, A. M. S., Tinkham, W. T., Roy, D. P., Boschetti, L., Kremens, R. L., Kumar, S. S., Sparks, A. M., & Falkowski, M. J. (2013). Quantification of fuel moisture effects on biomass consumed derived from fire radiative energy retrievals. *Geophysical Research Letters*, *40*(23), 6298–6302. https://doi.org/10.1002/2013GL058232

Stephens, S. L., Finney, M. A., & Schantz, H. (2004). Bulk density and fuel loads of ponderosa pine and white fir forest floors: Impacts of leaf morphology. *Northwest Science*, *78*(2), 93–100.

Stephens, S. L., Moghaddas, J. J., Edminster, C., Fiedler, C. E., Haase, S., Harrington, M., Keeley, J. E., Knapp, E. E., Mciver, J. D., Metlen, K., Skinner, C. N., & Youngblood, A. (2009). Fire treatment effects on vegetation structure, fuels, and potential fire severity in western U.S. forests. *Ecological Applications*, *19*(2), 305–320. https://doi.org/10.1890/07-1755.1

Swayze, N. C., Tinkham, W. T., Vogeler, J. C., & Hudak, A. T. (2021). Influence of flight parameters on UAS-based monitoring of tree height, diameter, and density. *Remote Sensing of Environment*, *263*, 112540. https://doi.org/10.1016/j.rse.2021.112540

Terryn, L., Calders, K., Åkerblom, M., Bartholomeus, H., Disney, M., Levick, S., Origo, N., Raumonen, P., & Verbeeck, H. (2022). Analysing individual 3D tree structure using the R package ITSMe. *Methods in Ecology and Evolution*, *00*, 1–11. https://doi.org/10.1111/2041-210X.14026

Tinkham, W. T., & Swayze, N. C. (2021). Influence of Agisoft Metashape Parameters on UAS Structure from Motion Individual Tree Detection from Canopy Height Models. *Forests*, *12*(2), 1–14. https://doi.org/10.3390/f12020250

Tseng, Y. H., & Wang, M. (2005). Automatic plane extraction from LIDAR data based on octree splitting and merging segmentation. *IEEE International Geoscience and Remote Sensing Symposium (IGARSS)*, *5*, 3281–3284. https://doi.org/10.1109/IGARSS.2005.1526542

USDA. (2022). *Confronting the wildfire crisis: a strategy for protecting communities and improving resilience in America's forests*. https://doi.org/FS-1187a

Valero, M. M., Verstockt, S., Butler, B., Jimenez, D., Rios, O., Mata, C., Queen, Ll., Pastor, E., & Planas, E. (2021). Thermal infrared video stabilization for aerial monitoring of active wildfires. *IEEE Journal of Selected Topics in Applied Earth Observations and Remote Sensing*, *14*, 2817–2832. https://doi.org/10.1109/JSTARS.2021.3059054

Van Wagtendonk, J. W., Sydoriak, W. M., & Benedict, J. M. (1998). Heat content variation of Sierra Nevada conifers. *International Journal of Wildland Fire*, *8*(3), 147–158. https://doi.org/10.1071/wf9980147

Varner, J. M., Gordon, D. R., Putz, F. E., & Kevin Hiers, J. (2005). Restoring fire to long-unburned Pinus palustris ecosystems: Novel fire effects and consequences for long-unburned ecosystems. *Restoration Ecology*, *13*(3), 536–544. https://doi.org/10.1111/j.1526-100X.2005.00067.x

Vega, C., Hamrouni, A., El Mokhtari, A., Morel, M., Bock, J., Renaud, J. P., Bouvier, M., & Durrieue, S. (2014). PTrees: A point-based approach to forest tree extraction from lidar data. *International Journal of Applied Earth Observation and Geoinformation*, *33*(1), 98–108. https://doi.org/10.1016/J.JAG.2014.05.001

Waring, K. M., Hansen, K. J., & Flatley, W. (2016). Evaluating prescribed fire effectiveness using permanent monitoring plot data: A case study. *Fire Ecology*, *12*(3), 2–25. https://doi.org/10.4996/FIREECOLOGY.1203002/TABLES/4

Watts, A. C., Perry, J. H., Smith, S. E., Burgess, M. A., Wilkinson, B. E., Szantoi, Z., Ifju, P. G., & Percival, H. F. (2010). Small unmanned aircraft systems for low-altitude aerial surveys. *Journal of Wildlife Management*, *74*(7), 1614–1619. https://doi.org/10.2193/2009-425

Weber, K. T., & Yadav, R. (2020). Spatiotemporal trends in wildfires across the Western United States (1950–2019). *Remote Sensing*, *12*(18), 2959. https://doi.org/10.3390/rs12182959

Whelan, A. W., Cannon, J. B., Bigelow, S. W., Rutledge, B. T., & Sánchez Meador, A. J. (2023). Improving generalized models of forest structure in complex forest types using area- and voxel-based approaches from lidar. *Remote Sensing of Environment*, *284*, 113362. https://doi.org/10.1016/J.RSE.2022.113362

White, J. C., Wulder, M. A., Vastaranta, M., Coops, N. C., Pitt, D., & Woods, M. (2013). The utility of image-based point clouds for forest inventory: A comparison with airborne laser scanning. *Forests*, *4*(3), 518–536. https://doi.org/10.3390/f4030518

Williams, C. J., Pierson, F. B., Nouwakpo, S. K., Al-Hamdan, O. Z., Kormos, P. R., & Weltz, M. A. (2020). Effectiveness of prescribed fire to re-establish sagebrush steppe vegetation and ecohydrologic function on woodland-encroached sagebrush rangelands, Great Basin, USA: Part I: Vegetation, hydrology, and erosion responses. *Catena*, *185*, 103477. https://doi.org/10.1016/j.catena.2018.02.027

Wooster, M. J. (2002). Small-scale experimental testing of fire radiative energy for quantifying mass combusted in natural vegetation fires. *Geophysical Research Letters*, *29*(21), 23–1. https://doi.org/10.1029/2002GL015487

Wooster, M. J., Roberts, G., Perry, G. L. W., & Kaufman, Y. J. (2005). Retrieval of biomass combustion rates and totals from fire radiative power observations: FRP derivation and calibration relationships between biomass consumption and fire radiative energy release. *Journal of Geophysical Research: Atmospheres*, *110*(D24), 1–24. https://doi.org/10.1029/2005JD006318

Wotton, B. M., Gould, J. S., McCaw, W. L., Cheney, N. P., & Taylor, S. W. (2012). Flame temperature and residence time of fires in dry eucalypt forest. *International Journal of Wildland Fire*, *21*(3), 270–281. https://doi.org/10.1071/WF10127